Construction and Building Materials 491 (2025) 142723

Contents lists available at ScienceDirect

Construction and Building Materials

journal homepage: www.elsevier.com/locate/conbuildmat

Sustainable utilization of corn husk ash as a pozzolanic cement substitute for mortar production

Behailu Zerihun Hailemariam [a], Mitiku Damtie Yehualaw [a], Woubishet Zewdu Taffese [b,c,*], Duy-Hai Vo [d]

[a] Faculty of Civil and Water Resource Engineering, Bahir Dar Institute of Technology, Bahir Dar University, Bahir Dar 6000, Ethiopia
[b] Department of Civil, Architectural and Environmental Engineering, Missouri University of Science and Technology, Rolla, MO 65401, USA
[c] School of Research and Graduate Studies, Arcada University of Applied Sciences, Jan-Magnus Jansson Aukio 1, Helsinki 00560, Finland
[d] Department of Materials Science and Engineering, Missouri University of Science and Technology, Rolla, MO 65401, USA

ARTICLE INFO

Keywords:
Corn husk ash
Durability
Eco-friendly mortar
Mechanical performance
Microstructure
Workability

ABSTRACT

In response to the global demand for low-carbon, energy-efficient, and sustainable construction materials, this study investigates the potential of corn husk ash (CHA) as a viable supplementary cementitious material (SCM) for partial cement replacement in mortar. CHA, derived from agricultural waste, was incorporated at 0–25 % replacement levels by weight of cement and thoroughly characterized for its chemical, physical, and mineralogical properties. With a combined SiO_2, Al_2O_3, and Fe_2O_3 content of 76.67 %, CHA satisfies ASTM Class N pozzolan requirements, demonstrating high pozzolanic reactivity. Although higher CHA content reduced workability—requiring 22 % more water and resulting in a 21 % slump reduction at 25 % replacement—significant improvements in long-term performance were observed. At 20 % CHA, the mortar achieved a dry density of 1908.84 kg/m^3 , 38.32 MPa compressive strength, and 4.38 km/s ultrasonic pulse velocity after 56 days. Durability was enhanced through reduced drying shrinkage, lower water absorption, improved acid resistance, and increased surface resistivity. Microstructural analysis revealed a denser matrix with refined pores, attributed to additional C–S–H formation via pozzolanic reactions. These results highlight CHA's potential as an eco-efficient alternative to cement, promoting greener construction. Further studies are recommended to explore its application in alkali-activated and geopolymer systems for broader structural use.

1. Introduction

Cement, the cornerstone of modern infrastructure, serves as the essential binder in cement paste, mortar, and concrete. However, its production is among the most energy-intensive industrial processes globally, demanding high thermal input and emitting substantial quantities of greenhouse gases [1,2]. This environmental footprint is largely attributed to the calcination of limestone during clinker production, which alone contributes approximately 0.87 tons of CO_2 per ton of cement manufactured [3,4]. Alarmingly, the cement industry accounts for nearly 8–9 % of global anthropogenic carbon dioxide emissions, making it one of the most pressing environmental challenges of the construction sector [5]. The U.S. Geological Survey reported that global cement production reached approximately 4.2 billion tons in 2017, with projections estimating a rise to 4.5 billion tons by 2050 [6]. This upward trajectory mirrors the rapid expansion of the global construction sector and underscores the urgent need for sustainable alternatives.

To mitigate this environmental burden, ambitious decarbonization strategies have emerged worldwide. One notable example is the European Cement Association's Net Zero Roadmap, a comprehensive vision for achieving carbon-neutral cement production by 2050 [7]. This roadmap emphasizes innovation across the cement–concrete lifecycle by targeting five interlinked areas—Clinker, Cement, Concrete, Construction, and Carbonation—popularly known as the five "C's." Such systemic interventions, while transformative, require complementary advancements in material science, particularly in sourcing eco-efficient cement substitutes.

Concurrently, the agricultural sector has experienced exponential growth. According to the U.S. Department of Agriculture and the

* Corresponding author at: Department of Civil, Architectural and Environmental Engineering, Missouri University of Science and Technology, Rolla, MO 65401, USA.
E-mail address: woubishet.taffese@arcada.fi (W.Z. Taffese).

https://doi.org/10.1016/j.conbuildmat.2025.142723
Received 10 May 2025; Received in revised form 11 July 2025; Accepted 13 July 2025
Available online 15 July 2025

Foreign Agricultural Service, global corn production surged by over 92 %, from 57.41 billion metric tons in 2010/11–110.49 billion metric tons in 2021/22 [8]. A significant byproduct of this growth is corn husk, the fibrous sheath encasing the corn cob, which is often discarded as waste despite its abundant availability and high lignocellulosic content. Data from the FAO estimate that corn husk constitutes approximately 20 % of the total corn weight, generating an estimated 117.8 million tons of waste in 2000 alone [9].

In light of growing concerns over solid waste accumulation due to urbanization, industrialization, and rapid construction, valorizing agricultural residues like corn husk ash (CHA) in cementitious systems offers a promising avenue for circular economy and low-carbon construction [10]. Numerous studies have successfully demonstrated the feasibility of utilizing agro-waste materials such as rice husk ash (RHA) [11,12], corn cob ash [13,14], and corn stalk ash [15,16] as partial cement replacements. Among these, CHA has recently emerged as a material of interest due to its high content of reactive silica, alumina, and iron oxides, aligning well with the chemical profile of Class N pozzolans [17,18,19,20].

Noteworthy investigations include the use of CHA in interlocking paving stones, where compressive strength increased with CHA content up to 10 %, and density remained comparable at CHA 15 % to that of 100 % OPC-based specimens at all curing phases [19]. Similarly, [18] and [20] reported marginal reductions in early-age compressive strength of CHA-blended mortars, but strength values at 56 days remained similar to the control mixes. Furthermore, [17] observed increased compressive strength in concrete with 2.5 %, 5 %, and 7.5 % replacements of corn leaf ash. Collectively, these studies suggest that CHA, particularly at replacement levels between 5 % and 15 %, can enhance or maintain compressive strength while offering a sustainable alternative to Portland cement.

Despite these promising preliminary results, there remains a critical gap in the comprehensive assessment of CHA's influence on the mechanical properties, microstructural characteristics, and long-term durability performance of mortar. Most existing studies are limited in scope, often focusing on early-age strength or isolated material parameters, without evaluating the holistic performance required for real-world structural applications.

This study introduces a systematic and in-depth investigation of corn husk ash as a sustainable cement substitute in mortar systems, targeting a wide array of performance metrics, including workability, mechanical strength, microstructure, and durability under various curing regimes. Unlike earlier studies that focused primarily on early-age strength or small-scale applications, this work offers a holistic evaluation of CHA-blended mortar, aiming to (i) identify the optimal replacement level of CHA, (ii) understand the underlying microstructural transformations via scanning electron microscope (SEM) and X-ray diffraction (XRD), and (iii) assess the long-term durability characteristics through water absorption and sulfate resistance tests.

By bridging the knowledge gap between agricultural waste valorization and cementitious composite performance, this research not only promotes the sustainable integration of CHA into mainstream construction materials but also contributes to global efforts in decarbonizing the construction industry. The findings of this study are expected to inform future material standards and policy frameworks for the utilization of agro-waste in sustainable infrastructure development.

2. Materials and methods

2.1. Materials used

In this study, Portland limestone cement (PLC) grade 42.5 R, obtained from Dangote Cement Factory, and CHA were employed as the primary binder materials for mortar production. The quality of PLC was verified in accordance with ASTM C 1084 [21], and its use adhered to the requirements outlined in ASTM C150 [22].

The corn husk, an agricultural byproduct, was sourced from the crop production farm at Arba Minch University, Ethiopia. Post-harvest, the husks were sun-dried for 7 days to ensure efficient combustion, consistent ash quality, and operational safety during incineration [23]. Pre-drying is critical, as moist husks lead to excessive energy consumption, incomplete combustion, and higher impurity levels, while also posing safety risks such as steam buildup, thermal shock, and particle spattering during rapid heating [24,25,26]

Once dried, the husks were incinerated in an electric furnace at 650 °C for 4 h to minimize unburnt carbon content and Loss on Ignition (LoI), as recommended by [19,27]. This temperature–time profile has also been validated in the context of calcining agricultural residues to produce ash suitable for cement replacement. For instance, [28] evaluated the chemical composition, weight loss, and strength activity index of rice husk ash (RHA), wheat straw ash (WSA), and cow dung ash (CDA) under varying calcination conditions. Their findings indicated that ashes calcined at 600 °C for durations between 2 and 6 h exhibited superior pozzolanic reactivity and mechanical performance. These results reinforce the suitability of the calcination conditions employed in the present study for producing high-quality pozzolanic CHA.

The resulting ash, characterized by a dark gray color, was finely ground using a Los Angeles abrasion testing machine, and the powder fractions passing through both 75 μm and 150 μm sieves were collected for use. The selected particle size range (75–150 μm) was governed by the mechanical limitations of the grinding equipment and the unavailability of finer milling technologies, which constrained the production of ultrafine CHA. The complete production process for CHA is illustrates in Fig. 1.

The physical properties and chemical compositions of PLC and CHA, determined through various test methods, as summarized in Table 1. The chemical compositions were performed using X-ray fluorescence (XRF) analysis. PLC and CHA had specific densities of 3.15 g/cm^3 and 2.38 g/cm^3 , respectively. CHA exhibited a Brunauer-Emmett-Teller (BET) surface area of 365.46 m^2/g, approximately 15 % higher than that of PLC (318 m^2/g), indicating its greater fineness and reactivity. As shown in Table 1 and the CaO-SiO_2-Al_2O_3 ternary diagram (Fig. 2), the XRF analysis of the binders indicates that the CHA is rich in SiO_2 (52.38 %) and Al_2O_3 (22.73 %), with appreciable amounts of MgO, CaO, K_2O, P_2O_5, and Fe_2O_3, minor constituents such as Na_2O, MnO, and TiO_2. The LoI of CHA was 4.75 %, within the permissible range. Based on the total content of SiO_2, Al_2O_3, and Fe_2O_3 (76.67 %) and LoI, CHA fulfills the chemical requirements for natural pozzolans outlined in ASTM C618 [29], qualifying it as a Class N pozzolan. These values are in line with previous studies [9].

The morphological characteristics of CHA and PLC were investigated using Scanning Electron Microscopy (SEM), as shown in Fig. 3. The SEM micrographs reveal that CHA particles exhibit angular, sharp-edged, and highly irregular geometries, with flat, coarse surfaces (Fig. 3**(a)**)—traits that suggest a high degree of surface reactivity. Additionally, the presence of a glassy and porous texture further underscores the material's pronounced pozzolanic potential. In contrast, the SEM image of PLC (Fig. 3**(b)**) illustrates a denser and more compact microstructure, characterized by granular particles of varying sizes and angular morphology.

X-ray Diffraction (XRD) analysis was also conducted to assess the mineralogical compositions of both materials, using a BRUKER D2 PHASER diffractometer with Cu Kα radiation across a 2θ range of 10°–60°. As illustrated in Fig. 4, the CHA sample predominantly consists of crystalline quartz (SiO_2), accompanied by minor phases including magnetite, calcite, hematite, and mullite. Conversely, the PLC sample shows well-defined peaks corresponding to clinker minerals such as alite (C_3S), belite (C_2S), and calcium carbonate (calcite), along with minor constituents like tricalcium aluminate (C_3A), tetracalcium aluminoferrite (C_4AF), and free lime.

To assess the microstructural characteristics of CHA, the Scherrer equation (Eq. (1)) was adopted to calculate the average crystallite size, while the crystalline index (CI) was determined using "Relative to Total

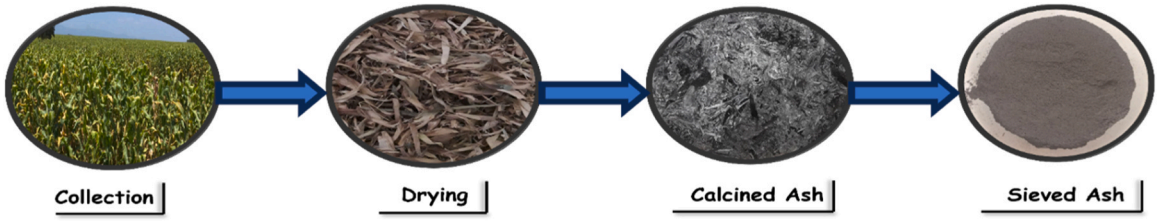

Fig. 1. Production process of corn husk ash.

Table 1
Physical properties and chemical compositions of PLC and CHA.

Description		Binding Materials	
		PLC	CHA
Physical properties	Specific density [g/cm^3]	3.15	2.38
	Surface area [m^2/g]	318	365.46
	Pore size [Å]	8.13	8.76
	Pore volume [cc/g]	0.08	0.08
	Color	Gray	Dark gray
Chemical compositions [%]	CaO	64	4.72
	SiO_2	22	52.38
	Al_2O_3	5.6	22.73
	Fe_2O_3	5.2	1.56
	MgO	1.98	5
	K2O	0.83	3.72
	P_2O_5	-	3.7
	Na_2O	0.54	0.24
	MnO	0.57	0.12
	TiO_2	-	0.07
	LoI	1.38	4.75
		Σ SiO_2+Al_2O_3+ Fe_2O_3	76.67

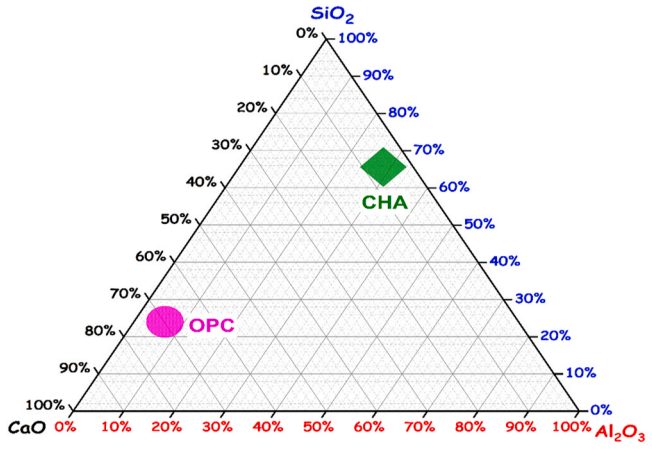

Fig. 2. CaO–SiO_2–Al_2O_3 ternary diagram of PLC and CHA.

Area" method (Eq. (2)) based on the XRD patterns [30,31]:

$$D = \frac{k * \lambda}{\beta co\theta}, \quad (1)$$

where, D = average crystallite size, k = shape factor (0.94), λ = X-ray wavelength, β = the full width at half maximum (FWHM) in radians, and θ = Bragg angle.

$$CI\ (\%) = A_{crystalline} / A_{total} \quad (2)$$

where, $A_{crystalline}$ = *sum of the areas under the crystalline peaks, and* A_{total} = total area including amorphous background.

The analysis revealed an average crystallite size of 44.48 nm a crystallinity index of 31 %, suggesting that the CHA is predominantly (69 %) amorphous. This level of amorphous content falls well within the effective range for high-amorphous Class N natural pozzolans (55–85 %), as reported in previous studies [32,33,34].

For mortar production, laboratory tap water and natural river sand from Konso area were used. The sand passing a 4.75 mm sieve, was washed and characterized per ASTM standards. Its properties, unit weight (1597 kg/m^3), specific gravity (2.64), absorption (2.54 %), and fineness modulus (2.38), fall within acceptable ranges for fine aggregates. The grading curve is illustrated in Fig. 5, and detailed properties are listed in Table 2.

2.2. Mix Proportions and Sample Preparations

To ensure consistency and comparability across all formulations, mortar specimens were prepared using a fixed cement-to-sand ratio of 1:2.75 by weight, in accordance with ASTM C 109 [39], which specifies proportions for standard 2-inch (50 mm) cube specimens. A constant water-to-binder (w/b) ratio of 0.48 was adopted throughout the study to maintain uniform workability and eliminate variability in performance that might arise from differences in water content.

To evaluate the effect of CHA, PLC was partially replaced with CHA in increments of 5 %, up to a maximum of 25 % by volume. This replacement was adjusted based on the optimal water content required for each mix, ensuring consistent consistency across all formulations. Table 3 outlines the detailed proportions of materials used to prepare 1 m^3 of mortar, accounting for a 25 % shrinkage factor. A control mix containing 100 % cement was also prepared for comparative purposes.

To ensure consistency in sample preparation, the binder materials (PLC and CHA) were first dry-mixed for two minutes at a low speed in a mechanical mixer with a capacity of 4.73 liters (5 quintals) at a speed of 20 rpm. After achieving a uniform dry mixture, the appropriate quantity of water was gradually added, and the mixture was blended for an additional five minutes at moderate speed to form a homogenous paste. Once the desired workability was confirmed through consistency tests, the mortar was cast into anti-corrosive metal molds of varying sizes, depending on the specific test to be performed. The mortar was carefully compacted in two layers using a table vibrator with a capacity of 3000–3600 rpm, to ensure uniformity and eliminate air pockets, a crucial step for evaluating the hardened properties accurately. After molding, the samples were allowed to set and dry in the molds for 24 h prior to demolded. To promote hydration and achieve optimal curing conditions, all specimens were stored in a water tank at an ambient temperature of 25°C ± 2°C for the designated curing periods. The specimens were cured for 3, 7, 28, and 56 days before being tested for their hardened properties, ensuring a comprehensive analysis of their performance over time.

In total, 111 mortar cubes were cast, with a minimum of three specimens prepared for each curing age to ensure statistical validity and result reliability. Except for those used in flexural strength and dry shrinkage tests, all specimens were cast in 5 × 5 × 5 cm cubic molds. Flexural strength tests employed 40 × 40 × 160 mm prism molds, while dry shrinkage tests utilized 25 × 25 × 285 mm prism molds.

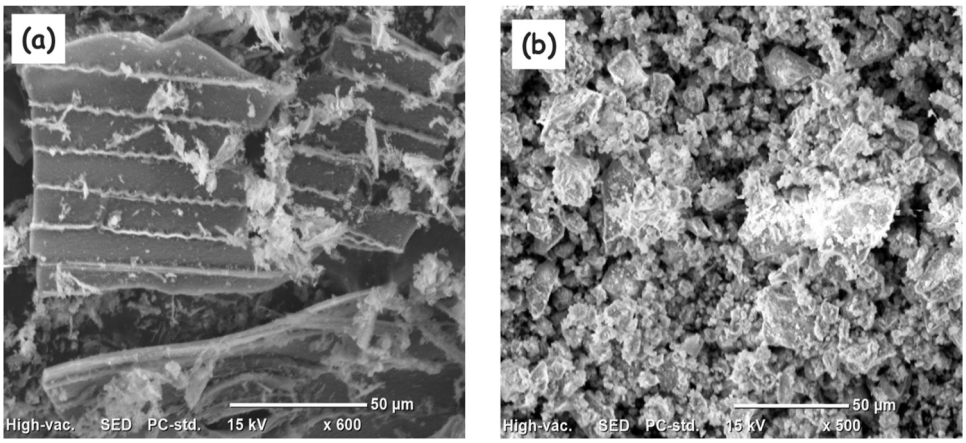

Fig. 3. SEM images of powders (a) CHA and (b) PLC.

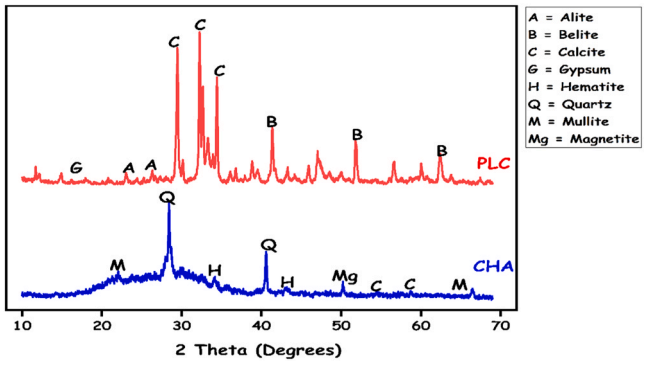

Fig. 4. XRD traces of CHA and PLC.

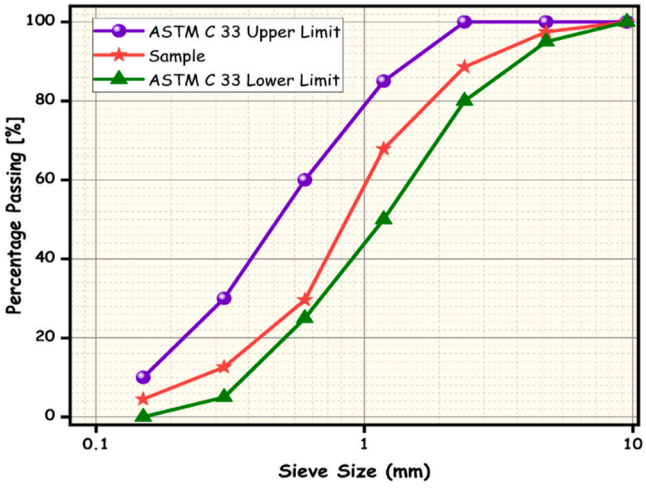

Fig. 5. Particle size distribution of the fine aggregate.

2.3. Experimental procedures

2.3.1. Workability tests

The initial stage of the study focused on evaluating the workability of the binder paste mixes using consistency and setting time, following ASTM C187 [40] and ASTM C191 [41], respectively. Besides, the slump flow test was conducted to further to investigate the flowability and workability of the mortars in accordance with ASTM C151/C151M [42]. These workability tests were essential to ensure the practicality of the mixes before casting and testing the hardened and microstructure properties.

Table 2
Physical properties and results of fine aggregate with respective test methods.

S. No.	Property	Test Methods	Result	Unit	Standard Value
1	Silt Content	ASTM C 40 [35]	4.17 %	[%]	Max., 8
2	Absorption or Bulking of Sand	ASTM C 128 [36]	2.54 %	[%]	Max., 3
3	Fineness Modulus	ASTM C 136 [37]	2.38	[-]	2.2–2.6
4	Moisture Content	ASTM C 566 [38]	5.38 %	[%]	2–6
5	Unit Weight	ASTM C 128 [36]	1597	[kg/m^3]	1520–1680
6	Specific Gravity	ASTM C 128 [36]	2.64	[-]	2.50–2.68

Table 3
Mix proportions of materials in 1 m^3 of CHA-based cement mortars.

Mix Code	Cement Content		CHA Content		Water	Sand
	Volume, [%]	wt, [kg]	Volume, [%]	wt, [kg]	[lit]	[kg]
CHA−0	100 %	566.67	0 %	0.00	272.00	1558.33
CHA−5	95 %	538.33	5 %	35.13	272.00	1558.33
CHA−10	90 %	510.00	10 %	56.67	272.00	1558.33
CHA−15	85 %	481.67	15 %	70.27	272.00	1558.33
CHA−20	80 %	453.33	20 %	140.53	272.00	1558.33
CHA−25	75 %	425.00	25 %	175.67	272.00	1558.33

2.3.2. Mechanical tests

Concurrent with the workability tests, the soundness of the cement pastes was assessed in accordance with ASTM C1437 [43]. Subsequently, a range of mechanical tests was conducted, including bulk dry density, compressive strength, flexural strength, and ultrasonic pulse velocity (UPV), to evaluate the mechanical performance of the mortars. The bulk dry density, compressive and flexural strength tests were conducted in accordance with ASTM C642 [44], ASTM C109 [39], and ASTM C348 [45], respectively; while the UPV test was performed bases on ASTM C597 [46].

2.3.3. Characterization of samples

For microstructural analysis, broken pieces from post-compressive strength testing were utilized. These samples were first immersed in ethanol (97 % purity) for 24 h to halt the hydration process. They were subsequently oven-dried at 105 ± 5°C for 24 h, as recommended by

[47]. The hydration products of the mortar specimens were assessed using SEM (JEOL model JSM-6390LV) after preparing small and thin slices (10 × 10 mm) from the broken mortar samples. These slices were not polished, but were coated with a platinum alloy for SEM analysis. The key hydration products that could be identified in the SEM analysis included calcium hydroxide (C–H), calcium silicate hydrate gel (C–S–H), ettringite, and unreacted particles and pore spaces.

In addition to SEM analysis, Fourier transform infrared spectroscopy (FTIR), X-ray diffraction (XRD), and thermogravimetric analysis (TGA) were employed to further investigate the microstructure of the mortar. After compressive strength testing, the specimens were immersed in ethanol solution and oven-dried, then crushed and ground to powders passing through a 75 μm (#200) sieve. The FTIR analysis aimed to identify chemical components in the samples, such as those observed in SEM, along with additional compounds like carbon and water. FTIR measurements were carried out using a DIGILAB FTS-3500 with a transmittance wavelength range of 400–4000 cm^{-1}, as described in [48].

TGA was employed to assess the thermal stability and mass loss resulting from temperature changes. The TGA analysis was performed using a PerkinElmer STA6000 machine with a temperature range of 40–800°C, with a heating rate of 20°C/5 min [49]. The results from TGA provided insights into the carbonation of calcium carbonate ($CaCO_3$), the dihydroxylation of C-S-H gel, and the dehydration of C–H gel, as described in [50,51].

2.3.4. Durability tests

The durability performance of the mortar samples was evaluated through water absorption, apparent porosity, sulfate resistance, drying shrinkage, and electrical surface resistivity (ESR) tests. Water absorption and porosity were determined using ASTM C642 [44] to assess permeability and pore structure. For sulfate resistance, mortar cubes were first cured in water for 24 h, then immersed in a 5 % magnesium sulfate ($MgSO_4$) solution for 3, 7, 28, and 56 days. This test was conducted in accordance with ASTM C1898 [52] and supplemented by procedures outlined in prior studies [53]. Resistance to sulfate attack was quantified through changes in compressive strength and mass relative to unexposed control specimens.

Drying shrinkage was measured in line with ASTM C157 [54], recording length changes from the initial reading before curing to subsequent values at 7, 28, 56, 91, and 120 days. Electrical surface resistivity was evaluated to assess the mortar's resistance to ionic penetration and potential durability in aggressive environments. This was done using a four-point Wenner probe with a 38 mm spacing, as described in AASHTO T277 [55].

3. Results and discussions

3.1. Fresh properties

3.1.1. Water demand and slump flow

Previous research reported that incorporating aro-waste materials as a partial or complete cement replacement influences the workability properties of cementitious systems [11]. In the present study, the impact of CHA on water demand and mortar workability is presented in Fig. 6. As shown, the inclusion of CHA in the binder system notably increased the water requirement of the mixes. For instance, the paste mix with a 25 % CHA replacement level exhibited a consistency of 33.07 %, in contrast to 27.04 % revealed for the reference PLC mix—representing an approximate 22 % increase in water demand. This behavior is primarily attributed to the hygroscopic nature and high surface area (365.46 m^2/g) compared to PLC (310 m^2/g). The porous, irregular texture of CHA (Fig. 3), along with the elevated free CaO content [56], further contributes to its higher water absorption capacity, thereby increasing the water requirement to achieve desirable workability. Moreover, the relationship between water demand and CHA

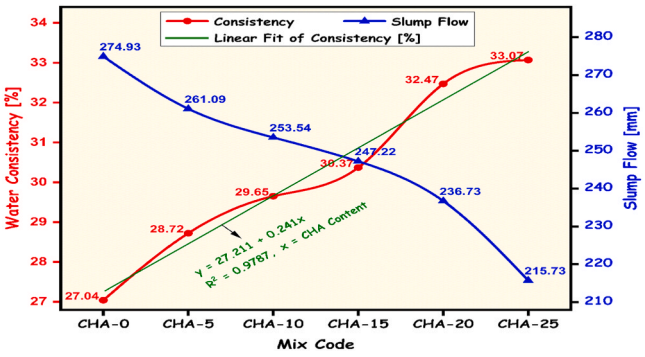

Fig. 6. Effect of CHA on water consistency and slump flow of cement paste.

replacement level exhibited a strong positive linear trend, with a coefficient of determination (R^2) of 0.9787, indicating a highly predictive correlation. Similar findings have been reported by [57], where the substitution of cement with 30 % sugarcane bagasse ash (SCBA) increased the w/b from 0.61 to 0.761, representing a 24.75 % rise to support hydration and pozzolanic activity.

In terms of slump flow, a consistent reduction in flowability was observed with increasing CHA content. The average slump flow values recorded for CHA level of 0 %, 5 %, 10 %, 15 %, 20 %, and 25 % were 274.93 mm, 261.09 mm, 253.54 mm, 247.22 mm, 236.73 mm, and 215.73 mm, respectively. This translates to reductions of approximately 8 %, 16 %, and 34 % for CHA-5, CHA-15, and CHA-25 mixes relative to the control (CHA-0). This reduction in slump could attributed the rough surface morphology, angularity, and porous of CHA particles, which increase internal friction which is responsible and hinder the flow of the fresh mortar [58]. Comparable findings were reported by [59], who observed a 4 % decrease in workability when cement was partially replaced with 20 % rice husk silica ash.

Further, literature indicates that mortars incorporating natural pozzolans with finer particle size distributions and higher specific surface areas typically exhibit greater reductions in slump flow, especially when used at low w/b ratios [60,61]. This behavior is consistent with the present study, where CHA fractions in the 75–150 μm range were used. As reported by [62], the use of such particle sizes can significantly reduce slump flow due to increased water demand and surface interaction, emphasizing the role of particle fineness in workability loss.

3.1.2. Setting time

The setting times of various binder formulations incorporating CHA are shown in Fig. 7. A clear trend of accelerated setting is observed as the

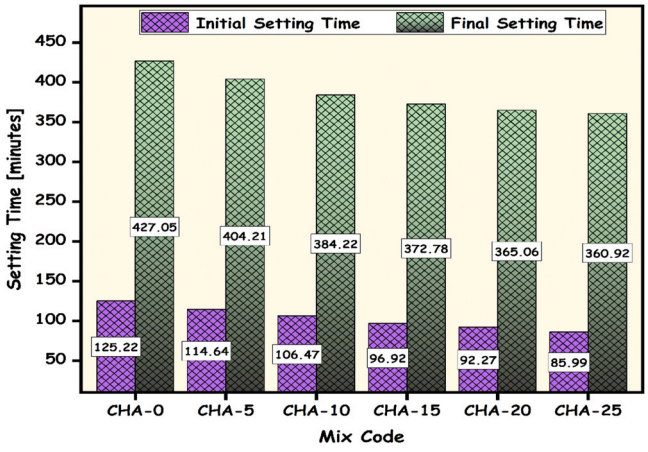

Fig. 7. Initial and final setting times of CHA -modified and control cement pastes.

CHA content increase from 5 % to 25 %. The control mix displayed the longest initial and final setting times, recorded at 125.22 min and 427.05 min, respectively. In contrast, the CHA-25 mix demonstrated a markedly faster setting behavior, initiating set at 85.99 min and completing final set at 360.92 min, approximately 15 % shorter than the control. This acceleration is largely due to the high fineness, amorphous silica, and elevated alumina content of CHA, which enhance the pozzolanic reactivity. These components react more readily with calcium hydroxide $Ca(OH)_2$, promoting the earlier formation of C-S-H gel, which contributes to quicker stiffening of the matrix. The findings align with prior studies indicating the role of reactive aluminosilicate phases in expediting setting times [63]. Interestingly, the setting behavior of CHA-5 was nearly identical to that of the control, attaining about 91 % and 95 % of the initial and final setting times, respectively. This suggested that low CHA substitutions have a negligible impact on setting kinetics. Importantly, all paste formulations conformed to the standard requirements of both ASTM and Ethiopian standards, confirming their suitability for practical application.

3.2. Mechanical performance

3.2.1. Soundness

Fig. 8 illustrates the influence of varying CHA content on the soundness of cement pastes. The result depicts that the incorporation of CHA enhances the paste resistance to volume changes at the time of setting and hardening. Remarkably, the CHA-20 mix attained the highest volumetric stability, registering an expansion of only 0.43 mm, a corresponding to an 87 % improvement over the control mix. This performance can be attributed to several synergistic factors: the pozzolanic reactivity of CHA reduces the amount of free CaO by facilitating secondary hydration reactions, while the balanced MgO content and micro-filling effect of CHA particles help limit capillary porosity and residual stress buildup [64].

Moreover, the soundness values display a strong correlation with CHA incorporation, indicated by a high coefficient of determination (R^2 = 0.9188), underscoring the reproducibility and reliability of the findings. All test results remain well within the limits prescribed by ASTM C151 [42], which stipulates a maximum allowable expansion of 10 mm for Portland cements.

3.2.2. Bulk dry density

Table 4 presents the evolution of bulk dry density in mortar specimens containing different proportions of CHA, monitored at 3, 7, 28, and 56 days. The results reveal that incorporating CHA significantly enhances the compaction and density of the hardened mortar. The control mix (CHA-0) had a 3-day density of 1531.19 kg/m^3, which increased steadily with curing age and CHA content. Notably, the CHA-20 mix consistently achieved the highest densities across all curing periods, reaching 1908.83 kg/m^3 at 56 days, a 24.66 % increase over the control. This enhancement is attributed to the formation of additional C-S-H gel formation due to pozzolanic activity of CHA, as well as the filler effect from its fine particle size and high specific surface area. These attributes facilitate better particle packing and reduced porosity, as supported by the microstructural observations. These findings affirm that CHA addition not only maintains the integrity of the hardened mortar but actively improves its structural compactness, aligning with previous literature [63].

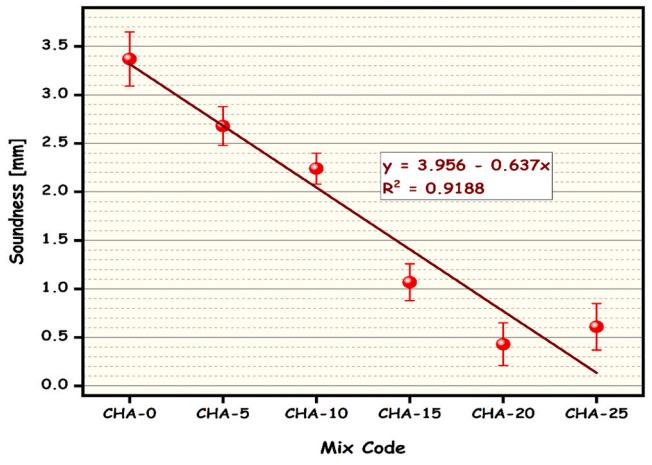

Fig. 8. Soundness of cement paste incorporating varying levels of CHA.

3.2.3. Compressive strength

The compressive strength development of CHA-blended cement mortar as a function of curing time and CHA replacement percentage is shown in Fig. 9. All mortar samples exhibited progressive strength gain over time, consistent with the ongoing hydration and pozzolanic reactions. The control mix achieved strengths of 13.83 MPa and 32.50 MPa at 3 and 56 days, respectively. Remarkably, the CHA-20 mix outperformed the control at all ages, achieving 23.78 MPa and 38.32 MPa—representing 72 % and 18 % enhancements at the 3rd and 56th days, respectively.

Furthermore, the CHA-25 mix also exhibited superior strength performance, confirming that optimal CHA inclusion levels fall between 20–25 %. At 28 days, compressive strength gains over the control were recorded as follows: CHA-5 (+0.72 MPa), CHA-10 (+2.57 MPa), CHA-15 (+4.41 MPa), CHA-20 (+6.50 MPa), and CHA-25 (+5.79 MPa). The enhancement is largely due to the abundant reactive silica in CHA, which accelerates the formation of secondary C-S-H gel, thereby improving the load-bearing capacity [65,66]. This trend is consistent with prior studies, such as [67], which documented similar performance using Guinean CHA. In contrast, other agro-waste ashes such as corn cob ash have demonstrated detrimental effects at higher replacement levels, with [68] reporting a 9.50 MPa reduction in compressive strength when cement was partially replaced with 20 % corn cob ash.

A statistically significant linear relationship was established between compressive strength, CHA content, and curing age, captured by the fitted equation: $f_c = 17.302 + 0.314a + 0.283b$, *where a is the CHA content (%) and b is the curing age (days),* with an adjusted $R^2 = 0.877$.

3.2.4. Flexural strength

Given that the incorporation of CHA in cement mortar enhanced the compressive strength, a corresponding improvement in flexural behavior was anticipated. Fig. 10 illustrates the flexural strength evolution of mortar samples incorporating varying CHA dosages. A linear enhancement in strength was observed with increasing CHA content up to a 25 % cement replacement, particularly evident at extended curing durations.

At 56 days, the flexural strength of CHA-modified mortars ranged between 5.55 MPa and 6.36 MPa, with the CHA-20 mix attaining the highest value of 6.36 MPa, followed closely by CHA-25 at 6.02 MPa. These values represent a 14.6 % and 8.6 % increase, respectively, over the control (CHA-0) mix. Furthermore, partial replacement of cement with CHA (0–25 %) yielded 48 –84 % and 10 –18 % improvements in flexural strength at 28 days compared to the 3-day and 7-day curing results, respectively. These enhancements are attributed to post-hydration pozzolanic activity that facilitates the formation of cross-linked C-S-H gel networks [69], the inherent hydrophilicity of CHA [70], and improved interfacial bonding within the mortar matrix [71]. Collectively, these factors lead to a denser microstructure and delayed-age strength gains. Notably, the CHA-20 and CHA-25 mixes exhibited superior synergy between hydration kinetics and microstructural refinement, mirroring findings by [12], who observed a > 16 % flexural gain using 20 % corn stalk ash replacement. Comparable studies also support this trend; for example, [72] reported that replacing cement with 10 % cashew leaf ash yielded 2.33 % and 2.2 % improvements in

Table 4
Bulk dry density of mortar mixes samples with varying CHA content.

Mix Code	Average Bulk dry density, [kg/m^3]				Increment of density compared to CHA-0, [%]			
	3rd day	7th day	28th day	56th day	3rd day	7th day	28th day	56th day
CHA−0	1531.19	1613.39	1682.03	1777.51	-	-	-	-
CHA−5	1555.74	1628.95	1732.83	1787.57	1.60 %	6.38 %	13.17 %	16.74 %
CHA−10	1558.17	1652.16	1759.21	1815.76	1.76 %	7.90 %	14.89 %	18.58 %
CHA−15	1644.35	1693.60	1788.43	1829.27	7.39 %	10.61 %	16.80 %	19.47 %
CHA−20	1703.42	1724.20	1830.65	1908.83	11.25 %	12.61 %	19.56 %	24.66 %
CHA−25	1682.84	1720.78	1792.71	1854.77	9.90 %	12.38 %	17.08 %	21.13 %

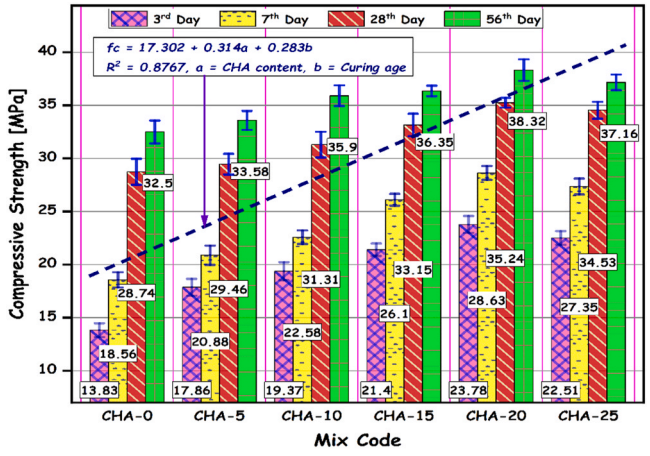

Fig. 9. Compressive strength development of cement mortar with varying CHA content at different curing ages.

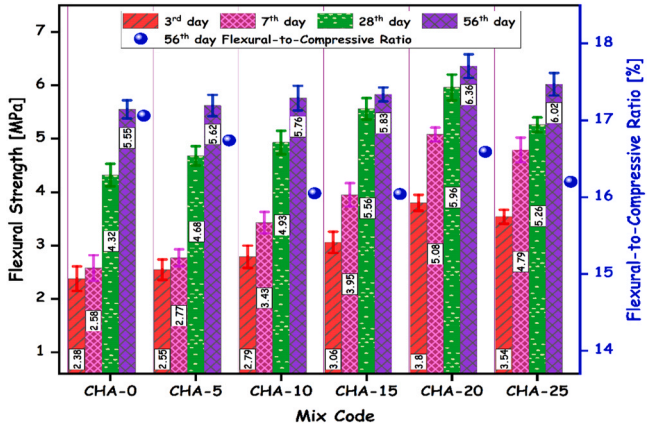

Fig. 10. Flexural strength development of PLC-CHA mortar mixes at different curing ages.

flexural strength at 56 and 90 days, respectively.

Additionally, Fig. 10 highlights the flexural-to-compressive strength ratios for 56-day cured samples, which ranged between 16.04 % and 17.06 %—well within and often exceeding international guideline thresholds. For instance, the CHA-20 mix achieved a ratio of 16.5 %, surpassing the laboratory testing results observed by BS EN 1015–11 [73], ASTM C 348 [74] and ASTM C 349 [75], all of which typically report ratios between 10–20 %. This underscores the structural efficiency and mechanical reliability of CHA-enhanced mortars for flexural applications.

3.2.5. Ultrasonic pulse velocity (UPV)

Fig. 11 displays the UPV measurements across various mortar mixes containing 0–25 % CHA at different curing ages. Results reveal a

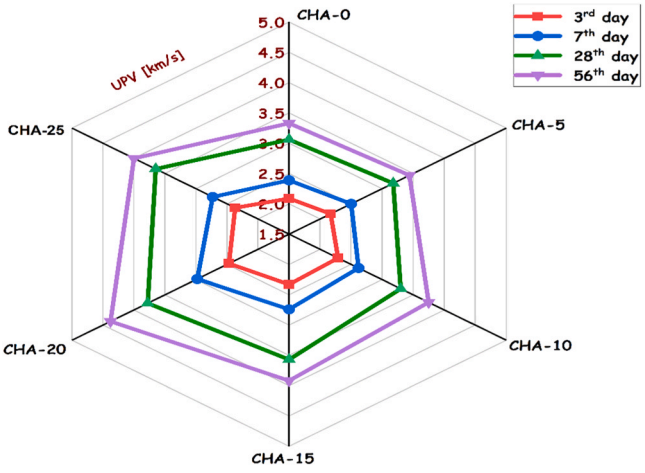

Fig. 11. Effect of CHA content on UPV of mortar samples across varying curing durations.

pronounced increase in UPV values with rising CHA content up to 20 %, particularly at later curing stages. At 56 days, UPV ranged from 3.06 km/s (CHA-0) to a peak value of 4.38 km/s for the CHA-20 mix, confirming superior internal quality and material densification. While the CHA-25 mix exhibited a marginal decline, its UPV values remained significantly higher than the control, reflecting a well-structured matrix. Remarkably, all 56-day UPV results—excluding the CHA-0 and CHA-5 samples—fell within the 'good' quality range (3.5–4.0 km/s) according to IS 13311 (Part 1) [76], with CHA-20 slightly exceeding this upper bound, indicating exceptional microstructural cohesion. Compared to the control mix, the CHA-20 mortar passed ultrasonic pulses 0.72 km/s (at 28 days) and 1.05 km/s (at 56 days) faster, validating its enhanced compactness and reduced void structure.

The densification observed in CHA-based mortars arises from several mechanisms, including: (i) accelerated pozzolanic reactions at later ages, (ii) transformation of macropores into mesopores via hydrotalcite (Ht) crystal precipitation [77], (iii) development of a refined interfacial transition zone (ITZ) [48], and (iv) the amorphous structure of CHA promoting secondary C-S-H gel growth [78]. These phenomena collectively contribute to the formation of a robust, compacted matrix with improved mechanical and durability characteristics. Fig. 12 further established a strong positive correlation ($R^2 = 0.9431$) between UPV and compressive strength, and a strong inverse relationship ($R^2 = 0.8843$) between UPV and apparent porosity.

3.3. Microstructure

3.3.1. Fourier-transform infrared (FTIR) spectroscopy

Fig. 13 **(a)** and **(b)** present the FTIR spectra of mortar specimens of the control mix (CHA-0), CHA-5, and CHA-20 cured for 7 and 28 days, respectively. On the 7th day (Fig. 13 **(a)**), prominent absorption bands were identified in the ranges of 490–1030 cm^{-1} , 1505–2375 cm^{-1} , and 2920–3840 cm^{-1} . A sharp peak near 490 cm^{-1} in CHA-5 was associated

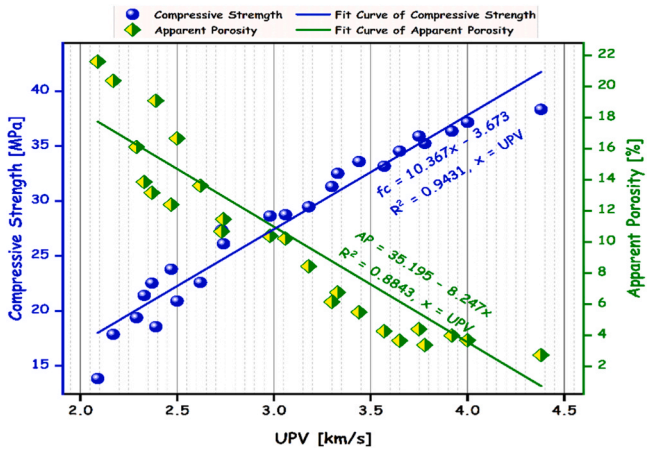

Fig. 12. Linear correlations between UPV and both compressive strength and apparent porosity.

with unhydrated iron oxide (Fe_2O_3) particles, while similar features in CHA-0 and CHA-20 around 500 cm^{-1} suggested the formation of unreacted alite and belite—linked to delayed strength development in earlier-age hydration [48,79]. Peaks at 940–955 cm^{-1} confirmed the formation of C–S–H gel via Si-O asymmetric stretching, with a shift toward 1030 cm^{-1} in CHA-20 indicating enhanced silica crystallization. Asymmetric stretching of sulfate groups (SO_4^{2-}) from gypsum and ettringite was evident between 1090 and 1192 cm^{-1} [80].

The presence of $CaCO_3$ and H_2O was observed around 1510 cm^{-1} in CHA-5, with slightly reduced intensities at 1505 cm^{-1} in CHA-0 and CHA-20. Methylene (C–H) stretching from CH_2/CH_3 groups appeared distinctly near 2370–2375 cm^{-1} in all samples. Notably, O-H-O vibrations of absorbed water emerged near 2920–2925 cm^{-1}, shifting according to CHA content. Broad O-H bands 3550–3840 cm^{-1} indicated C-H formation, with band intensity increasing with CHA dosage, suggesting more extensive hydration reactions.

At 28 days (Fig. 13 **(b)**), similar spectral features were retained, affirming ongoing hydration and phase development. The persistent bands at 490–500 cm^{-1} and 935–1030 cm^{-1} further indicated continued formation of unreacted phases and C-S-H gel. CHA-0 exhibited stronger $CaCO_3$ and CH^- related bands at 1510 cm^{-1} and 2360 cm^{-1}, respectively, attributed to enhanced CO_3^{2-} and CH–group presence [80]. Broadened O–H stretching near 2910–2925 cm^{-1} confirmed the inclusion of OH^- ions. Interestingly, CHA-20 demonstrated stronger C-H absorption and broader bands between 3550–3840 cm^{-1}, suggesting a greater degree of hydration product formation. These findings align with the assertion of [81] that hydrogen bonding becomes more prominent near 3700 cm^{-1} and above, indicating advanced curing and material transformation.

3.3.2. *Phase compositions of the mortar samples*

The phase evolution of cementitious systems incorporating CHA was comprehensively using X-ray diffraction (XRD) analysis. Fig. 14 illustrates the diffraction patterns of mortar specimens cured for 7 and 28 days, highlighting the mineralogical phases developed throughout the hydration process. At 7 days of curing, the control mix (CHA-0) predominantly displayed hydration products typical of ordinary Portland cement, including calcium hydroxide (C-H) in the form of portlandite (P), alite (C_3S), ettringite (AFt), and gypsum as monosulfate (AFm) mode, alongside a notable amount of C-S-H gel. Notably, the absence of CHA resulted in no crystalline silica (quartz) phases, corroborating findings from previous studies [80]. The pronounced diffraction peaks indicate a substantial quantity of portlandite, ettringite, gypsum, and alite, signifying active hydration. In contrast, the incorporation of CHA into the mortar mixes (CHA-5 and CHA-20) introduced crystalline quartz, with increasing peak intensity from CHA-5 to CHA-20. Peaks at 2θ values of 26.7° and 28° correspond to SiO_2 and C-H, respectively, confirming the ash's contribution to the overall phase composition. Alite, essential for early strength development, exhibited higher intensities than belite (C_2S) and C-S-H across all mixes, particularly in the early hydration stages. Both belite and C-S-H gel were identified in the 2θ region between 49.8° and 57.4°, whereas ettringite and gypsum were consistently detected around 18° in all mortar types.

XRD patterns of CHA-5 and CHA-20 at 28 days revealed prominent peaks for quartz and portlandite, while C-S-H and belite displayed broader, less intense humps, characteristic of their semi-crystalline or amorphous nature. C-S-H gel was notably detected at 2θ angles of 24°, 34.2°, 39.4°, 49.7°, and 57.5°, whereas C-H appeared at 28.2° and 29.6°, and belite was identified around 32° and 46.1°. The intensity of SiO_2 peaks (26.7° and 28.8°) in CHA-5 and CHA-20 mixes further confirmed

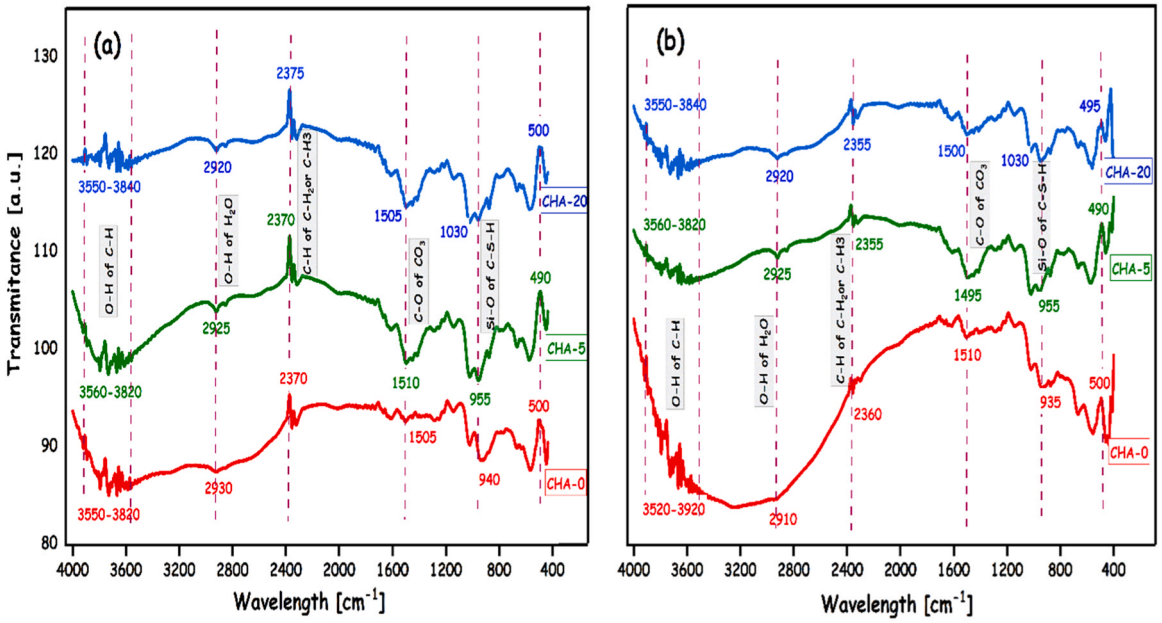

Fig. 13. FTIR spectra of mortar specimens containing CHA after (a) 7 days and (b) 28 days of curing.

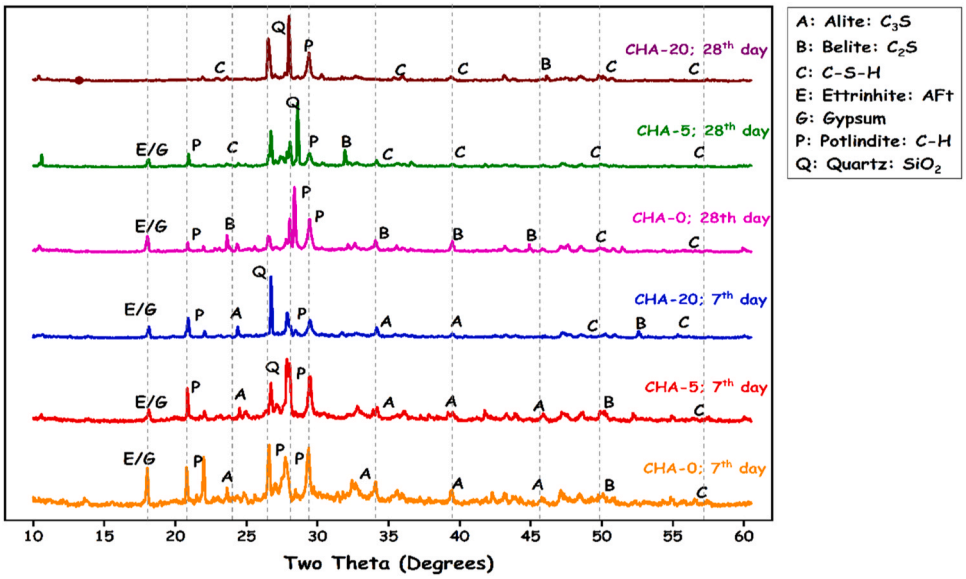

Fig. 14. XRD patterns CHA-containing mortar specimens cured at 7 and 28 days.

the increased crystalline silica presence due to CHA addition.

A quantitative summary of the hydration product content, determined using the Scherrer equation (Eq. (1) and **(2)**), is presented in Table 5. The control mix exhibited the highest C-H and alite content at early age, whereas CHA-5 and CHA-20 demonstrated significantly increased proportions of C-S-H gel over time, reflecting enhanced pozzolanic activity. While some CHA particles remained unreacted, particularly at higher replacement levels, these particles contributed positively through a filler effect, promoting matrix densification and refined pore structure. Notably, the concentrations of ettringite and gypsum decreased with extended curing, particularly in CHA-20, indicating their conversion into more stable hydration phases such as monosulfate and additional C–S–H. This transformation supports improved long-term durability and dimensional stability of the cementitious matrix by reducing the potential for deleterious expansion, shrinkage, and crack formation over time.

The substantial rise in C-S-H content and concurrent reduction of portlandite in CHA-rich mixes underscore the effectiveness of CHA in promoting pozzolanic reactions. These transformations ultimately result in a more refined and compact microstructure, as also evidenced by SEM investigations. As a consequence, the inclusion of CHA enhances the long-term mechanical performance of mortar by reducing porosity and increasing the volume of binding phases [82,83].

3.3.3. *Scanning electron microscope (SEM) analysis*

Fig. 15 and Fig. 16 present the SEM micrographs of CHA-0, CHA-5, and CHA-20after 7 and 28 days of curing, respectively. As noted in prior research [48,82], the predominant hydration products observable under SEM include C-S-H gel, C-H, ettringite, and AFm, alongside residual unreacted particles and pore structures, which are influenced by the binder chemistry and hydration kinetics. At the early stage of hydration (7 days, Fig. 15), the microstructure of CHA-0 revealed scattered formations of fibrous C-S-H gel embedded within a matrix abundant in crystalline calcium hydroxide and elongated needle-like ettringite. The presence of considerable porosity was evident, indicative of an immature and loosely packed matrix. However, the incorporation of CHA (CHA-5 and CHA-20) resulted in a visibly altered morphology: a more heterogeneous texture emerged, with a noticeable presence of unreacted CHA particles and denser hydration products. While the pozzolanic activity of CHA may not be fully activated at early ages, its filler effect clearly contributed to refining the microstructure, reducing pore size, and initiating nucleation sites for further C-S-H development [84].

After 28 days of curing (Fig. 16), the micrographs showcased pronounced microstructural evolution. he CHA-0 mix exhibited further development of C-S-H and C-H phases, but retained some degree of porosity. In stark contrast, the CHA-containing mortars displayed a substantially denser and more cohesive matrix. Especially in the CHA-20 mix, the microstructure appeared highly compacted with a well-interlocked network of C-S-H gel and significantly reduced pore space. This densification is attributed to the delayed yet vigorous pozzolanic reaction between the amorphous silica in CHA and free calcium hydroxide, leading to the secondary generation of additional C-S-H, which filled voids and enhanced the structural integrity of the mortar matrix [84]. The fineness and high glassy-phase content of CHA (as indicated in Table 1) further accelerated these processes by enhancing the surface area available for reaction and facilitating ion mobility [85]. This synergy between physical filler effects and chemical pozzolanic activity culminated in a robust microstructure, minimizing porosity and boosting mechanical performance, in alignment with findings from [86].

Table 5
Quantitative phase composition of hydration products in CHA-containing mortar specimens.

Hydration Products	Composition [%]					
	7th day			28th day		
	CHA-0	CHA-5	CHA-20	CHA-0	CHA-5	CHA-20
Portlandite (C-H)	32.01	22.2	13.35	19.06	6.22	5.22
Alite (C_3S)	26.98	14.07	6.57	0.00	0.00	0.00
Belite (C_2S)	11.30	2.85	1.30	10.78	2.00	2.00
Unreacted CHA	0.00	6.83	8.75	0.00	14.98	15.15
Ettringite and Gypsum (Aft/Afm)	4.65	3.11	3.39	3.48	1.81	0.00
C-S-H Gel	25.06	50.94	66.64	66.68	74.99	77.63

3.3.4. *Thermogravimetric analysis (TGA)*

TGA was conducted to assess the thermal stability and phase decomposition of mortar specimens containing varying amounts of CHA. The TGA curves shown in Fig. 17 **(a)** and **(b)** illustrate the mass loss during profiles of the samples at 7 and 28 days of curing, respectively, as the temperature increased from 20 to 800 °C. Each sample, with an initial mass of approximately 10 mg, underwent weight loss due to the decomposition of hydration products and mineral phases. Based on established studies [48,87], the mass loss in the TGA profiles can be

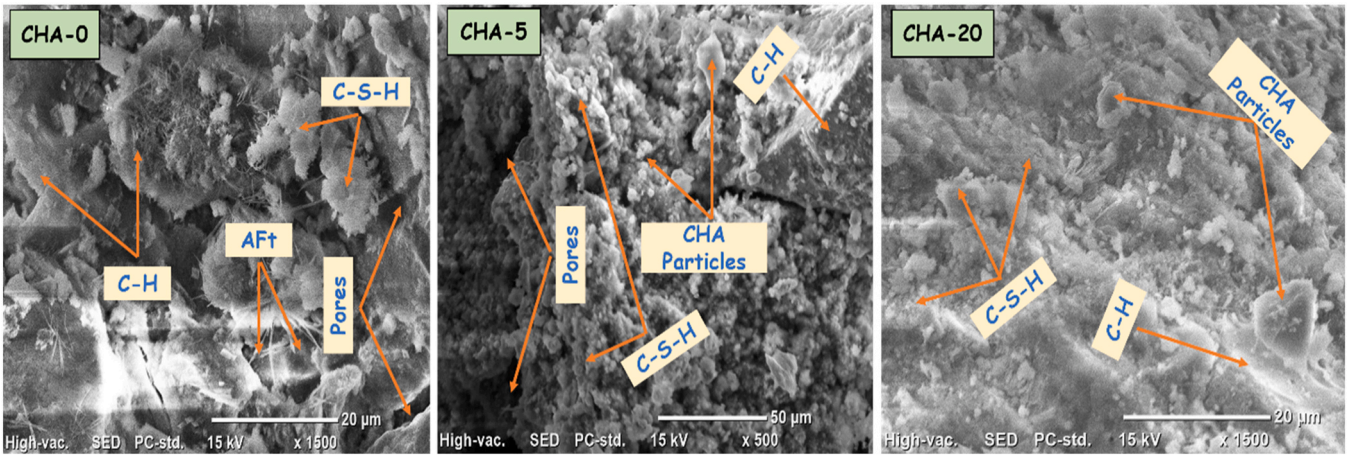

Fig. 15. SEM micrographs of mortar specimens cured for 7 days.

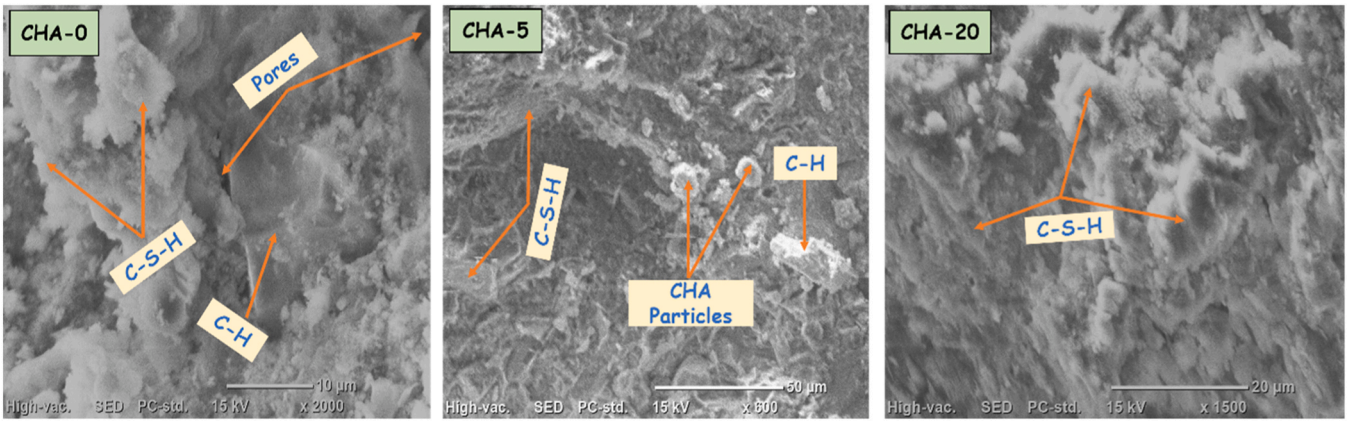

Fig. 16. SEM micrographs of mortar specimens cured for 28 days.

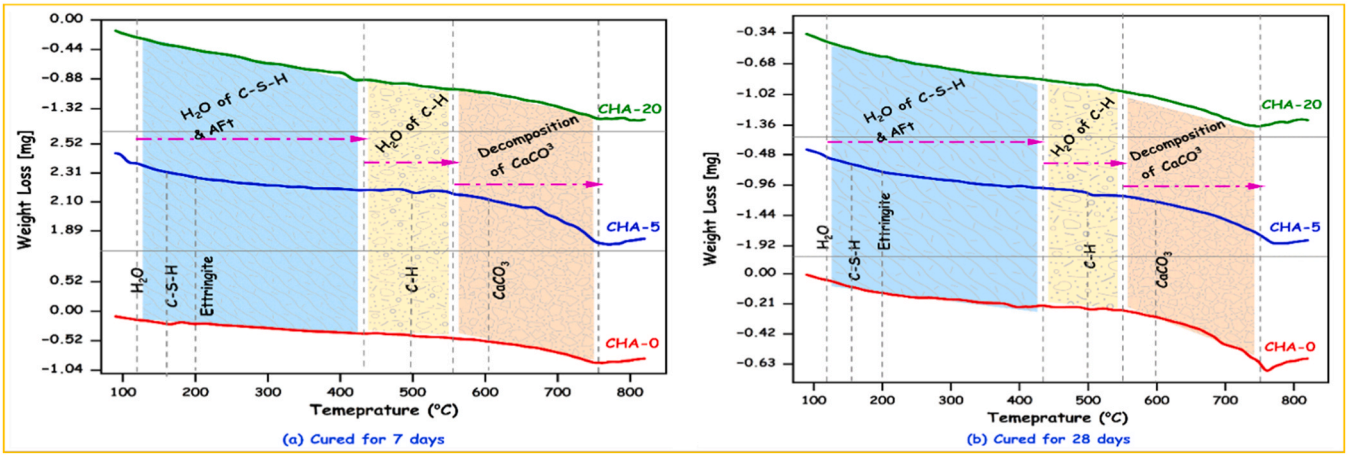

Fig. 17. TGA analysis of cement-CHA-based mortar after 7 and 28 days of curing.

categorized into three distinct temperature ranges: (1) 105–420 °C–loss of physically bound water and dehydration of C-S-H and ettringite; (2) 420–550 °C–dehydroxylation of calcium hydroxide (portlandite); and (3) 550–750 °C–decarbonation of calcium carbonate ($CaCO_3$) into calcium oxide (CaO) and CO_2.

At 7 days (Fig. 17 **(a)**), all mixes exhibited an initial mass loss below 120 °C, primarily attributed to the evaporation of unbound water. Notably, CHA-0 experienced a higher mass loss (2.38 mg) compared to CHA-5 (0.27 mg) and CHA-20 (0.15 mg), reflecting a more porous matrix with higher free moisture content. However, this stage alone may not accurately reflect the formation of C-S-H, as suggested by [84]. A significant mass reduction, averaging 15 %, was observed around 420 °C in all mixes, signaling the dehydration of C-S-H gel and AFt. As the temperature approached 550 °C, dehydroxylation of portlandite begin, with CHA-0 showing the greatest mass loss—indicative of lower thermal resistance. In contrast, CHA-5 and CHA-20 demonstrated enhanced

thermal stability, underscoring the protective effect of CHA incorporation on the matrix. The improved thermal performance is further highlighted in the 550–750 °C range, where CHA-based mortars exhibited more pronounced $CaCO_3$ decomposition, consistent with their higher calcite content confirmed by XRD results. Beyond 600 °C, mass loss accelerated, but CHA-5 and CHA-20 mixes retained greater stability, offering 36 % and 40 % higher resistance, respectively, than the CHA-0 mix.

The 28-day TGA results (Fig. 17 **(b)**) revealed even more pronounced differences in thermal behavior. CHA-0 displayed substantial mass loss in the 220–420 °C and 600–750 °C ranges, corresponding to the breakdown of C-H and decarbonation of $CaCO_3$. Conversely, CHA-5 and CHA-20 exhibited markedly reduced weight loss during these phases. Specifically, CHA-5 showed 10 %, 11.35 %, and 17.52 %, improved thermal stability at key degradation temperatures, confirming its progressive enhancement over time. Above 750 °C, CHA-20 exhibited a highly resilient structure, likely due to a dense and consolidated matrix rich in secondary C-S-H gel. This increased thermal resistance can be attributed to the lower portlandite content in CHA-blended mortars, a direct consequence of pozzolanic activity that consumes $Ca(OH)_2$ to form additional C-S-H [30]. The superior thermal behavior of CHA-20, showing 17.58 % greater stability than CHA-0, reaffirms its higher pozzolanic reactivity and enhanced cementitious performance [88]. Furthermore, [84] cautions that uncontrolled carbonation of portlandite can affect long-term durability—an issue mitigated by CHA through its portlandite-reducing effect.

In summary, both the 7-day and 28-day TGA profiles clearly validate the improved thermal stability and structural integrity of CHA-based mortars. These findings are consistent with SEM and XRD analyses, highlighting the pozzolanic consumption of C-H and the evolution of a denser microstructure in the order of CHA-20 > CHA-5 > CHA-0. The results not only substantiate the mechanical performance improvements observed but also underline the thermal resilience gained through CHA incorporation.

3.4. Durability properties

3.4.1. Water absorption

Fig. 18 presents the water absorption performance of hardened cement mortar incorporating varying percentages of CHA. As displayed, water absorption decreased consistently with higher CHA content, indicating an enhancement in mortar durability across all curing periods. The measured absorption values ranged from 3.02 % to 18.66 %. Mortars blended with 20 % and 25 % CHA demonstrated superior durability, achieving notably low water absorption rates of 3.02 % and 3.26 % at 56 days, respectively.

In comparison to the CHA-20 mix, the control specimens significantly higher water absorption, recording increases of 28 % at 3 days, 27 % at 7 days, 48 % at 28 days, and 57 % at the 56 days. Regardless of replacement level, the mean water absorption values were approximately 16.11 %, 14.00 %, 7.57 %, and 4.94 % at 3, 7, 28, and 56 days, respectively, as shown by the trend line in Fig. 18. These results align with previous studies reporting that the partial substitution of cement with agricultural waste-based SCMs—such as CHA [67], corn cob ash [14,13], and corn stalk ash [16,89]—significantly enhances durability. The improvement is mainly attributable to the unique pore-filling capacity and cohesive characteristics of these fine SCMs, which lead to a more refined and impermeable microstructure.

3.4.2. Void (air) space or apparent porosity

In parallel with the trends observed for bulk dry density and water absorption, the apparent porosity of mortar mixes decreased as the CHA content increased up to 20 %, followed by a slight increment at 25 %, across all hydration ages (Fig. 19). The void content reduction was most significant in mortars with 20 % CHA, exhibiting the lowest porosity of 2.73 % at 56 days, indicating a notably dense and compacted microstructure, with a similar trend observed for the CHA-25 specimens.

Porosity decreased following the order: CHA-0 > CHA-5 > CHA-10 > CHA-15 > CHA-25 > CHA-20. Mortars containing 20 % CHA showed improvements in microstructural densification by 42 %, 45 %, 67 %, and 60 % at 3, 7, 28, and 56 days, respectively, compared to the control. However, at 56 days, the apparent porosity of CHA-25 mortars exhibited a modest 35 % compared to CHA- 20, suggesting a threshold beyond which excessive CHA content may slightly compromise microstructural integrity. These observations are consistent with the chemically bound water content variations during hydration. The enhancement in microstructure is primarily attributed to the pozzolanic reaction and hydraulic diffusion of CHA particles into capillary voids, effectively sealing pores and producing a denser matrix [13,51]. In addition, the linear fit analysis indicates a moderate inverse correlation (R^2 = 0.783) between CHA incorporation and porosity for mortars immersed in water for 56 days.

3.4.3. Change in compressive strength due to sulfate attack

The resistance of cement mortars containing CHA against sulfate attack was assessed through measurements of compressive strength loss (Fig. 20 **(a)**) and weight loss (Fig. 20 **(b)**) after curing either water or in a 5 % $MgSO_4$ solution for 3, 7, 28, and 56 days. It was observed that all mortar mixes exhibited varying degrees of deterioration when exposed to the sulfate solution, particularly after 28 and 56 days of curing.

The control mix (CHA-0) exhibited the highest deterioration, with a

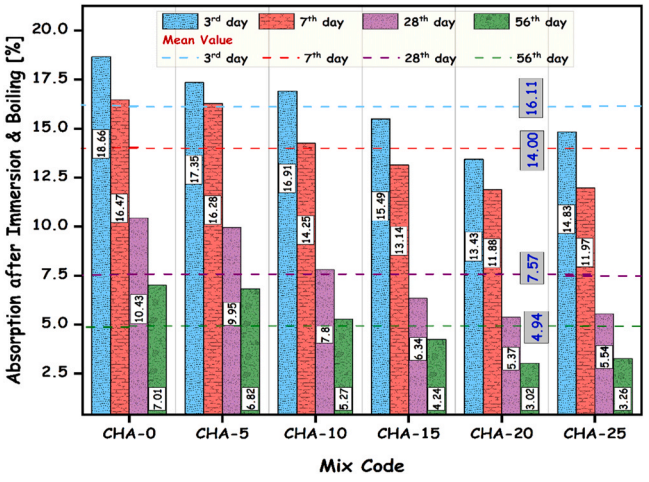

Fig. 18. Water absorption of CHA-containing mortar mixes after immersion and boiling.

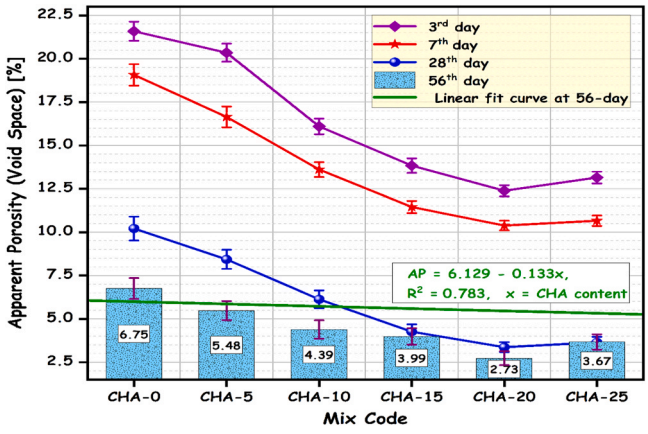

Fig. 19. Apparent porosity of mortar mixes as influenced by CHA content and curing duration.

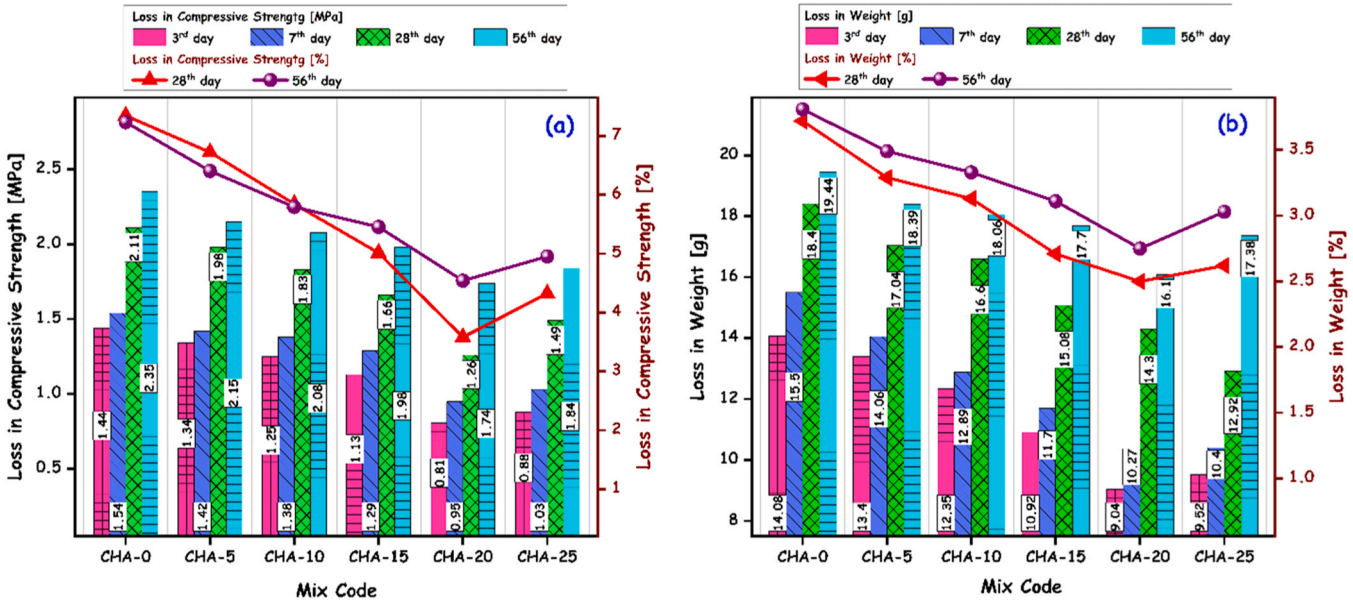

Fig. 20. Effect of CHA on sulfate attack in mortars (a) Loss in compressive strength and (b) Loss in weight.

7.3 % loss in compressive strength at 28 days and a 20 g weight loss by 56 days—demonstrating its vulnerability to sulfate-induced damage. In contrast, CHA-modified mortars, especially CHA-20 and CHA-25, displayed superior durability characteristics. Compressive strength losses across all mixtures ranged between 0.81 MPa and 2.35 MPa, while corresponding weight losses varied from 9.04 g to 19.44 g, as shown in Fig. 20 **(a)** and **20 (b)**.

At the 28 and 56 days, the CHA-20 mortar achieved approximately 29 % and 22 % greater resistance to compressive strength loss compared to the control, along with improvements of 30 % and 11 % in mass stability, respectively. Interestingly, increasing CHA content beyond 20 % did not lead to adverse effects under sulfate exposure; instead, it maintained or enhanced resistance without significant degradation. For instance, CHA-25 recorded the lowest mass loss (12.8 g at 56 days), translating to a minimal 2.7 % reduction in weight, while its strength reduction remained comparably low at 1.0 MPa (or ~3.5 %). These improvements can be attributed to several interrelated mechanisms. The inclusion of CHA contributes to pore structure refinement, limiting ionic ingress and alkali migration, which are critical precursors for sulfate attack. The lower CaO content in CHA (refer to Table 1) also plays a pivotal role by minimizing the formation of expansive reaction products such as gypsum and ettringite, thereby enhancing dimensional stability [51,90,91]

Additionally, the relationship between water absorption and sulfate resistance was examined using a linear fit, as shown in Fig. 21. The analysis revealed a strong inverse correlation between water consistency and loss in compressive strength (R^2 = 0.9325) and between water consistency and loss in weight (R^2 = 0.9049) at 28 and 56 days. This finding further confirms that mortars with reduced water absorption exhibited superior resistance to sulfate-induced degradation.

3.4.4. Dry shrinkage

Fig. 22 **(a)** and **(b)** appear illustrate effect of CHA content, ranging from 0 % to 25 % by weight of cement, on the length change of different mortar formulations due to dry shrinkage over curing periods from 7 to 120 days. As moisture loss tends to be greater at later ages, partly due to ongoing exothermic pozzolanic reactions [92,93], all mortar specimens exhibited increased shrinkage with time. The reference mortar made with 100 % of cement (CHA-0) showed a length change ranging from 2.00 × 10^{-3} cm at 7 days to 20.80 × 10^{-3} cm at 120 days. In contrast, mortars incorporating CHA displayed lower shrinkage values, ranging

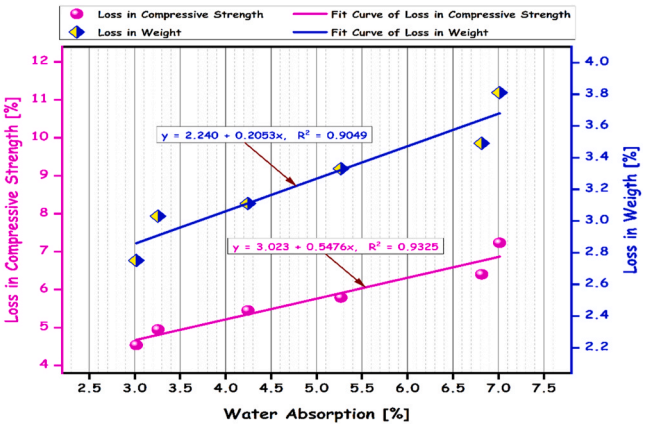

Fig. 21. Correlation between water absorption and sulfate resistance at 28 and 56 days.

from 0.86 to 18.53 × 10^{-3} cm over the same period (Fig. 22 **(a)**).

According to [94], substantial shrinkage observed after 91st and 120th days could be attributed factors such as the absence of crystal phases such as CH, the characteristics of C-A-S-H, relative humidity conditions, and the specific size distribution of pores. Overall, the incorporation of CHA into the mortars effectively reduced their susceptibility to shrinkage. The greatest shrinkage resistance was observed for the mix containing 20 % CHA. At hydration periods of 56, 91, and 120 days, the CHA-20 mortar retained 26.70 % (3.42 × 10^{-3} cm), 33.33 % (5.98 × 10^{-3} cm), and 35.61 % (7.41 × 10^{-3} cm) lower shrinkage, respectively, compared to the control. Notably, the performance of CHA-25 was comparable to that of CHA-20.

The mechanisms contributing to reduced shrinkage in CHA-modified mortars may involve several factors: the presence of unhydrated particles [89], the formation of a thin Na_2O film over hydration products that acts as a sealing barrier against moisture evaporation, and a reduction in capillary pressure gradients within the micropore network [49,94]. Additionally, the slight increase in capillary tension within the matrix may help push particles closer together, mitigating volumetric contraction. According to ASTM C157 [54], the permissible range for 28-day drying shrinkage is between 0.05 % and 0.06 %. As shown in Fig. 22 **(b)**, dry shrinkage values for all mortar formulations at 56, 91,

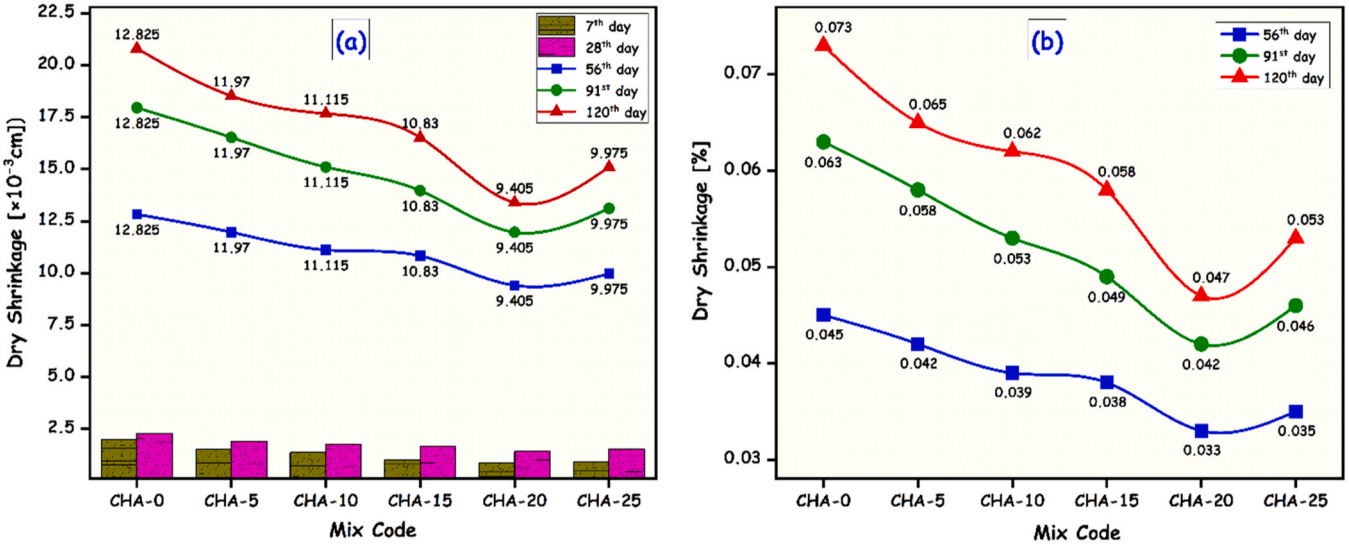

Fig. 22. Dry shrinkage behavior of mortar samples with varying CHA continents: (a) length change (in $\times 10^{-3}$ cm) and (b) shrinkage percentage.

and 120 days remained close to or within this acceptable limit.

3.4.5. *Electric surface resistivity (ESR)*

Fig. 23 demonstrates the average ESR result for mortar cubes cured for 7, 28, 56, and 91 days. As shown, the ESR values of the mortar mixes increased with both higher CHA content and longer curing durations, ranging from 8.23 to 14.57 KΩ.cm at 7 days and exceeding 79 KΩ.cm at 91 days for mortar incorporating 20 % CHA, which recorded the highest value among all mixes. At 28 and 56 days, the CHA-20 samples demonstrated significantly denser microstructures than the control samples, with corresponding ESR values of 11.20 and 17.86 KΩ.cm, respectively. This improvement in microstructure contributed to a reduced incidence of corrosion and enhanced the overall mortar durability. Furthermore, when compared to the control mix, mortar samples incorporating 5 %, 15 %, and 25 % exhibited ESR increases of 7.29 %, 16.08 %, and 19.62 %, respectively. According to [27], a minimum ESR value of 20 KΩ.cm is recommended for high-performance concrete (HPC) as an indicator of "good" durability. Accordingly, all mortar samples cured for more than 28 days in a water tank met this durability threshold. The enhancement in ESR with CHA addition can be attributed to the pozzolanic reactions occurring at later ages between CHA and PLC, resulting in the formation of a dense and interconnected C-S-H gel network. This denser structure reduces capillary porosity and chemical diffusion pathways [27,95]. Moreover, higher CHA contents likely diminish the mobility of leaching ions (such as Ca^{2+}, Na^{+}, K^{+}, and OH^{-}), which are primary conductors in cementitious materials. The increased consumption of free CH rough pozzolanic activity also reduces the availability of leachable Ca^{2+} and OH^{-} ions, contributing further to the enhanced electric resistivity [96].

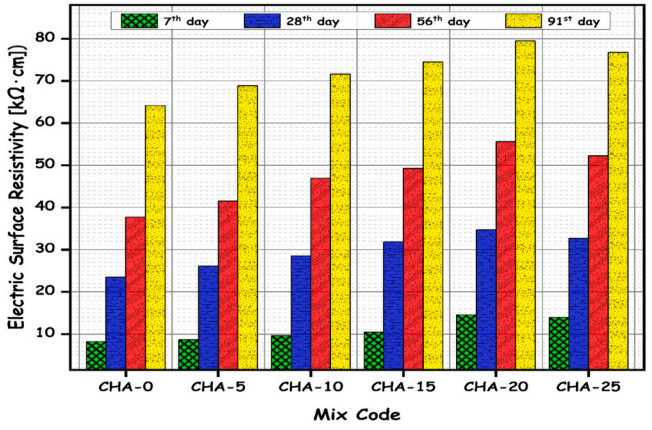

Fig. 23. Influence of CHA on the ESR of CHA-containing mortar samples.

4. Conclusions

This study evaluated the potential of CHA as a partial cement replacement in mortar, focusing on fresh, mechanical, durability, and microstructural performance. CHA, predominantly composed of silica (52.38 %) with 61 % amorphous content and crystalline quartz, meets the criteria for Class N pozzolans per ASTM C618. Its high reactivity led to significant improvements in strength and durability. Incorporating CHA reduced workability and setting time due to its high surface area and porous texture; however, at 20 % replacement, the mortar achieved optimal performance with a 56-day compressive strength of 38.32 MPa and flexural strength of 6.36 MPa. Enhanced microstructural densification, attributed to secondary C-S-H formation, contributed to reduced porosity, water absorption, shrinkage, and improved resistance to acid and sulfate attack. These results confirm CHA's effectiveness in improving mortar performance while promoting sustainable reuse of agricultural waste.

Despite these promising results, the study is limited to CHA as a sole cement replacement material and was conducted under controlled laboratory conditions. Broader performance under real-world exposure and structural application was not examined. In addition, synergistic effects with other supplementary cementitious materials (SCMs), as well as economic, environmental, and life-cycle assessments, were beyond the scope of this work, limiting comprehensive evaluation of CHA's practical and ecological impact.

To further advance this line of research, future investigations should incorporate comparative assessments between CHA and other pozzolanic materials to better contextualize its performance. Evaluating CHA's behavior in conjunction with other SCMs and within alkali-activated or geopolymer binders may reveal synergistic benefits. Long-term durability testing—including resistance to chloride ingress, carbonation, freeze-thaw cycles, and other aggressive exposures—is also essential to validate CHA's reliability in diverse climates and applications. Moreover, scaling up to industrial production, coupled with cost-effectiveness analyses and life-cycle sustainability assessments, will be vital for supporting CHA's practical deployment in mainstream construction.

CRediT authorship contribution statement

Duy-Hai Vo: Writing – review & editing, Validation, Supervision, Investigation, Conceptualization. **Behailu Zerihun Hailemariam:** Writing – original draft, Visualization, Validation, Software, Methodology, Investigation, Formal analysis, Data curation, Conceptualization. **Mitiku Damtie Yehualaw:** Writing – review & editing, Validation, Supervision, Resources, Project administration, Formal analysis, Conceptualization. **Woubishet Zewdu Taffese:** Writing – review & editing, Validation, Supervision, Investigation, Formal analysis, Conceptualization.

Declaration of Competing Interest

The authors declare that they have no known competing financial interests or personal relationships that could have appeared to influence the work reported in this paper.

Data availability

No data was used for the research described in the article.

References

[1] J.K. Prusty, S.K. Patro, S.S. Basarkar, Concrete using agro-waste as fine aggregate for sustainable built environment – a review, Int. J. Sustain. Built Environ. 5 (2) (2016) 312–333, https://doi.org/10.1016/j.ijsbe.2016.06.003.

[2] E.M. Getachew, B.W. Yifru, M.D. Yehualaw, The use of ground recycled concrete cement as an eco-friendly alternative cement material in mortar production, Iran. J. Sci. Technol. Trans. Civ. Eng. (2024), https://doi.org/10.1007/s40996-024-01606-3.

[3] D.M. Nega, B.W. Yifru, W.Z. Taffese, Y.K. Ayele, M.D. Yehualaw, Impact of partial replacement of cement with a blend of marble and granite waste powder on mortar, Appl. Sci. 13 (15) (2023), https://doi.org/10.3390/app13158998.

[4] S.A. Endale, W.Z. Taffese, D.H. Vo, M.D. Yehualaw, Rice husk ash in concrete, Sustain 15 (1) (2023), https://doi.org/10.3390/su15010137.

[5] K.M. Liew, A.O. Sojobi, L.W. Zhang, Green concrete: prospects and challenges, Constr. Build. Mater. 156 (2017) 1063–1095, https://doi.org/10.1016/j.conbuildmat.2017.09.008.

[6] D. Wang, C. Shi, N. Farzadnia, Z. Shi, H. Jia, Z. Ou, A review on use of limestone powder in cement-based materials: Mechanism, hydration and microstructures, Constr. Build. Mater. 181 (2018) 659–672, https://doi.org/10.1016/j.conbuildmat.2018.06.075.

[7] CEMBUREAU: European Cement Association, "From Ambition to Deployment - The Road Travelled, Pathways and Levers To Scale Up Our Net Zero Ambition," p. 131, 2024, [Online]. Available: ⟨https://cembureau.eu/library/reports/cembureau-s-net-zero-roadmap/⟩.

[8] B. Dukhnytskyi, World agricultural production, Ekon. APK (7) (2019) 59–65, https://doi.org/10.32317/2221-1055.201907059.

[9] A.A. Raheem, S.I. Adedokun, E.A. Adeyinka, B.V. Adewole, Application of corn stalk ash as partial replacement for cement in the production of interlocking paving stones, Int. J. Eng. Res. Afr. 30 (2017) 85–93, https://doi.org/10.4028/www.scientific.net/JERA.30.85.

[10] N. Sathiparan, A. Anburuvel, V.V. Selvam, Utilization of agro-waste groundnut shell and its derivatives in sustainable construction and building materials – a review, J. Build. Eng. 66 (January) (2023) 105866, https://doi.org/10.1016/j.jobe.2023.105866.

[11] B. Zerihun, M.D. Yehualaw, D.H. Vo, Effect of Agricultural Crop Wastes as Partial Replacement of Cement in Concrete Production, Adv. Civ. Eng. 2022 (2022), https://doi.org/10.1155/2022/5648187.

[12] I.S. Agwa, O.M. Omar, B.A. Tayeh, B.A. Abdelsalam, Effects of using rice straw and cotton stalk ashes on the properties of lightweight self-compacting concrete, Constr. Build. Mater. 235 (2020), https://doi.org/10.1016/j.conbuildmat.2019.117541.

[13] N. Bheel, A. Adesina, Influence of Binary Blend of Corn Cob Ash and Glass Powder as Partial Replacement of Cement in Concrete, Silicon 13 (5) (2021) 1647–1654, https://doi.org/10.1007/s12633-020-00557-4.

[14] S. Oyebisi, A. Ede, F. Olutoge, S. Ogbiye, Evaluation of reactivity indexes and durability properties of slag-based geopolymer concrete incorporating corn cob ash, Constr. Build. Mater. 258 (2020) 119604, https://doi.org/10.1016/j.conbuildmat.2020.119604.

[15] Q. Li, et al., Effect of waste corn stalk ash on the early-age strength development of fly ash/cement composite, Constr. Build. Mater. 303 (July) (2021) 124463, https://doi.org/10.1016/j.conbuildmat.2021.124463.

[16] A.M. Maglad, M. Amin, A.M. Zeyad, B.A. Tayeh, I.S. Agwa, Engineering properties of ultra-high strength concrete containing sugarcane bagasse and corn stalk ashes, J. Mater. Res. Technol. 23 (2023) 3196–3218, https://doi.org/10.1016/j.jmrt.2023.01.197.

[17] M. Aswin, E.S. Maranatha, L. Nola, Effect of use of corn leaf ash on concrete compressive strength, IOP Conf. Ser. Mater. Sci. Eng. 1122 (1) (2021) 012026, https://doi.org/10.1088/1757-899x/1122/1/012026.

[18] R. Ahumada, H. Ospina-Mateus, K. Salas-Navarro, Use of the rice and corn husk ashes as an innovative pozzolanic material in ceramic tile adhesive production, Procedia Comput. Sci. 198 (2021) (2022) 572–577, https://doi.org/10.1016/j.procs.2021.12.288.

[19] A. Shuaibu, et al., Optimum Portland Cement-Guinea Corn Husk Ash Blend as Filler in Hot Mix Asphalt Self-healing Concrete View project Optimum Portland Cement-Guinea Corn Husk Ash Blend as Filler in Hot Mix Asphalt, Covenant J. Eng. Technol. 4 (2) (2020). ⟨https://www.researchgate.net/publication/362890144⟩ ([Online]. Available).

[20] S.O. Odeyemi, O.D. Atoyebi, E.K. Ayo, Effect of Guinea Corn Husk Ash on the Mechanical Properties of Lateritic Concrete, IOP Conf. Ser. Earth Environ. Sci. 445 (1) (2020), https://doi.org/10.1088/1755-1315/445/1/012034.

[21] American Society for Testing & Materials, ASTM C 1084 - Standard Test Method for Portland-Cement Content of Hardened Hydraulic-Cement, Astm i (March 1997) (2015) 315–319, https://doi.org/10.1520/C1084-19.2.

[22] American Society for Testing & Materials, ASTM C 150/C 150M - standard test method for portland cement, Astm (August 2021) (2021).

[23] S. Yuan, Y. Hou, S. Liu, Y. Ma, A comparative study on rice husk, as agricultural waste, in the production of silica nanoparticles via different methods, Mater. (Basel) 17 (6) (2024) 1–11, https://doi.org/10.3390/ma17061271.

[24] M. Saito, K. Amagai, G. Ogiwara, M. Arai, Combustion characteristics of waste material containing high moisture, Fuel 80 (9) (2001) 1201–1209, https://doi.org/10.1016/S0016-2361(00)00208-8.

[25] S. Islamova, A. Tartygasheva, J. Karaeva, V. Panchenko, Y. Litti, A comprehensive study on the combustion of sunflower husk pellets by thermogravimetric and kinetic analysis, kriging method, Agric 13 (4) (2023), https://doi.org/10.3390/agriculture13040840.

[26] X. Meng, R. Sun, T.M. Ismail, W. Zhou, X. Ren, R. Zhang, Parametric studies on corn straw combustion characteristics in a fixed bed: Ash and moisture content, Energy 158 (2018) 192–203, https://doi.org/10.1016/j.energy.2018.06.060.

[27] D.-H. Vo, C.-L. Hwang, K.-D. Tran Thi, M.D. Yehualaw, W.-C. Chen, Effect of fly ash and reactive MgO on the engineering properties and durability of high-performance concrete produced with alkali-activated slag and recycled aggregate, J. Mater. Civ. Eng. 32 (11) (2020) 04020332, https://doi.org/10.1061/(asce)mt.1943-5533.0003420.

[28] S. Zaffar, A. Kumar, N.A. Memon, R. Kumar, A. Saand, Investigating optimum conditions for developing pozzolanic ashes from organic wastes as cement replacing materials, Mater. (Basel) 15 (6) (2022) 1–15, https://doi.org/10.3390/ma15062320.

[29] American Society for Testing & Materials, ASTM C 618 - standard specification for coal fly-ash and raw or calcined natural pozzolan for use in concrete, Astm 08 (March 2023) (2023) 3–4, https://doi.org/10.1520/C1709-18.

[30] F.T.L. Muniz, M.A.R. Miranda, C. Morilla Dos Santos, J.M. Sasaki, The Scherrer equation and the dynamical theory of X-ray diffraction, Acta Crystallogr. Sect. A Found. Adv. 72 (3) (2016) 385–390, https://doi.org/10.1107/S205327331600365X.

[31] A. Monshi, M.R. Foroughi, M.R. Monshi, Modified Scherrer Equation to Estimate More Accurately Nano-Crystallite Size Using XRD, World J. Nano Sci. Eng. 02 (03) (2012) 154–160, https://doi.org/10.4236/wjnse.2012.23020.

[32] B.I. Djon Li Ndjock, J. Baenla, J.B.B. Mbah, A. Elimbi, M. Cyr, Amorphous phase of volcanic ash and microstructure of cement product obtained from phosphoric acid activation, SN Appl. Sci. 2 (4) (2020) 1–10, https://doi.org/10.1007/s42452-020-2496-7.

[33] Y.K. Cho, S.H. Jung, Y.C. Choi, Effects of chemical composition of fly ash on compressive strength of fly ash cement mortar, Constr. Build. Mater. 204 (2019) 255–264, https://doi.org/10.1016/j.conbuildmat.2019.01.208.

[34] Y. Wei, G. Dong, B. Fang, G. Wang, Understanding reactive amorphous phases of fly ash through the acidolysis, Cem. Concr. Compos 140 (2023) 105102, https://doi.org/10.1016/j.cemconcomp.2023.105102.

[35] American Society for Testing & Materials, ASTM C 150/C 150M - Standard Specification for Portland Cement, in: Astm, i, 2021, pp. 3–5, doi: 10.1520/C0117-17.10.1520/C0117-23.2.

[36] American Society for Testing & Materials, "ASTM C 128 - Standard Test Method for Relative Density (Specific Gravity) and Absorption of Fine Relative Density (Specific Gravity) and Absorption of Fine Aggregate Aggregate," Astm, 2015, doi: 10.1520/C0128–22.1.

[37] American Society for Testing & Materials, ASTM C 136/C 136M - standard test method for seive analysis of fine and coarse aggregates, Astm (January) (2019) 1–2, https://doi.org/10.1520/C0136.

[38] American Society for Testing & Materials, ASTM C 566 - standard test method for total evaporation moisture content of aggregate by drying, Astm i (Reapproved) (2018) 3–5, doi: 10.1520/C0566-97R04.10.1520/C0566-13.2.

[39] American Society for Testing & Materials, ASTM C 109 - standard test method for compressive strength of hydraulic cement mortars (Using 2-in. or [50 mm] Cube Specimens), Astm 04 (2021) 1–7, https://doi.org/10.1520/C0109.

[40] American Society for Testing & Materials, ASTM C 187 - standard test method for normal consistency of hydraulic cement, Astm i (C) (2021) 1–3.

[41] American Society for Testing & Materials, ASTM C 191 - standard test methods for time of setting hydraulic cement by vicat needle, Astm 9 (1) (2003) 1–6, https://doi.org/10.1520/C0191-21.2.

[42] American Society for Testing & Materials, ASTM C 151 - Standard Test Method for Autoclave Expansion of Hydraulic Cement, Astm i (Jan 2015) (2018) 3–5, https://doi.org/10.1520/C0150.

[43] American Society for Testing & Materials, ASTM C 1437 - standard test method for flow of hydraulic cement mortar, Astm (2001) 7–8, https://doi.org/10.1520/C1437-20.2.

[44] American Society for Testing & Materials, ASTM C 642 - standard test method for density, absorption, and voids in hardened concrete, Astm 08 (Reapproved 1989) (2000) 3–4, https://doi.org/10.1520/C1709-18.

[45] American Society for Testing & Materials, ASTM C 348 - standard test method for flexural strength of hydraulic-cement mortar, Astm 04 (April 2021) (2021) 1–5, doi: 10.1520/C0348-20.10.1520/C0348-21.2.

[46] American Society for Testing & Materials, ASTM C 597 - standard test method for ultrasonic pulse velocity through concrete, Asian J. Energy Environ. i (Reapproved) (2018) 3–5, doi: 10.1520/C0597-16.10.1520/C0597-22.2.

[47] P.C. Hewlett, Lea's Chemistry of Cement and Concrete, Elsevier Ltd, 2006.

[48] B.Z. Hailemariam, M.D. Yehualaw, W.Z. Taffese, D.H. Vo, Optimizing Alkali-Activated Mortars with Steel Slag and Eggshell Powder, Buildings 14 (8) (2024), https://doi.org/10.3390/buildings14082336.

[49] D. Vo, C. Hwang, K.T. Thi, M. Damtie, "Effect of polymer latex on the efflorescence, drying shrinkage and microstructure of alkali- activated slag paste,", J. Sustain. Cem. Mater. 0 (0) (2022) 1–11, https://doi.org/10.1080/21650373.2022.2079020.

[50] M.D. Yehualaw, M. Alemu, B.Z. Hailemariam, D. Vo, Aquatic weed for concrete sustainability, Sustain 14 (23) (2022) 15501.

[51] M.A. Worku, W.Z. Taffese, B.Z. Hailemariam, M.D. Yehualaw, Cow dung ash in mortar: an experimental study, Appl. Sci. 13 (10) (2023) 1–15, https://doi.org/10.3390/app13106218.

[52] American Society for Testing & Materials, "ASTM C 1898 - Standard Test Methods for Determining the Chemical Resitance of Concrete Products to Acid Attack," Astm, no. Stage I, pp. 9–10, 2020, doi: 10.1520/D1898–20.1.

[53] M.K. Baddoura, S.D. Aliyan, and W. Choeb, "Acid Resistance, Water Permeability and Chloride Penetrability of Concrete Containing Crushed Basalt as Aggregates," vol. 5, pp. 285–304, 2015, doi: 10.17265/2161-6213/2015.7-8.005.

[54] American Society for Testing & Materials, ASTM C 157/C 157M - standard test method for length change of hardened cement mortar and concrete, Astm (August 2017) (2017) 1–4, https://doi.org/10.1520/C0157.

[55] A. A. of S. H. and T. Officials, "AASHTO T 277 - Standard Method of Test for Electrical Indication of Concrete's Ability to Resist Chloride Ion Penetration Technically Revised: 2023 Editorially Revised: 2023 Technical Subcommittee: 3c, Hardened Concrete American Association of State," Aashto, pp. 22–24, 2023.

[56] E.M. Getachew, B.W. Yifru, W.Z. Taffese, M.D. Yehualaw, Enhancing mortar properties through thermoactivated recycled concrete cement, Buildings 13 (9) (2023), https://doi.org/10.3390/buildings13092209.

[57] P. Jagadesh, A. Ramachandramurthy, R. Murugesan, T. Karthik Prabhu, Adaptability of sugar cane bagasse ash in mortar, J. Inst. Eng. Ser. A 100 (2) (2019) 225–240, https://doi.org/10.1007/s40030-019-00359-x.

[58] M. Rafieizonooz, J. Mirza, M. Razman, M. Warid, E. Khankhaje, Investigation of coal bottom ash and fly ash in concrete as replacement for sand and cement, Constr. Build. Mater. 116 (2016) 15–24, https://doi.org/10.1016/j.conbuildmat.2016.04.080.

[59] E. Marangon, et al., Mortars produced with an environmentally sustainable rice HUSK silica: Rheological properties, J. Clean. Prod. 287 (2021) 125561, https://doi.org/10.1016/j.jclepro.2020.125561.

[60] T.Y. Wang, H.Y. Tsai, S.L. Hung, C.C. Jian, Research on engineering properties of cement mortar adding stainless steel reduction slag and pozzolanic materials, Case Stud. Constr. Mater. 16 (2020) e01144, https://doi.org/10.1016/j.cscm.2022.e01144.

[61] L. Turanli, B. Uzal, F. Bektas, Effect of large amounts of natural pozzolan addition on properties of blended cements 35 (2005) 1106–1111, https://doi.org/10.1016/j.cemconres.2004.07.022.

[62] Y. Zhao, J. Gao, C. Liu, X. Chen, Z. Xu, The particle-size effect of waste clay brick powder on its pozzolanic activity and properties of blended cement, J. Clean. Prod. 242 (2020) 118521, https://doi.org/10.1016/j.jclepro.2019.118521.

[63] M.V.A. Florea, Z. Ning, H.J.H. Brouwers, Activation of liberated concrete fines and their application in mortars, Constr. Build. Mater. 50 (2014) 1–12, https://doi.org/10.1016/j.conbuildmat.2013.09.012.

[64] E.M. Getachew, B.W. Yifru, B.T. Habtegebreal, M.D. Yehualaw, Performance evaluation of mortar with ground and thermo-activated recycled concrete cement, Cogent Eng. 11 (1) (2024), https://doi.org/10.1080/23311916.2024.2357726.

[65] C. Hwang, M. Damtie, D. Vo, T. Huynh, and A. Largo, "Performance evaluation of alkali activated mortar containing high volume of waste brick powder blended with ground granulated blast furnace slag cured at ambient temperature," vol. 223, pp. 657–667, 2019.

[66] E. Khankhaje *et al.*, "On blended cement and geopolymer concretes containing palm oil fuel ash," vol. 89, pp. 385–398, 2016.

[67] O.M. Raheem, A.A. Adedokun, S.I. Uthman, Q.A. Adeyemi, A.O. Oyeniyi, Application of Corn Husk Ash as Partial Replacement for Cement in the Production of Interlocking Paving Stones, LAUTECH J. Civ. Environ. Stud. 1 (1) (2018) 4–10, https://doi.org/10.36108/laujoces/8102/10(0130)A.

[68] A.B. Oriola, K.O. Raheem, A.A. Ogundele, Investigation of compressive strength and thermal properties of corn cob ash cement concrete, Mater. Today Proc. 86 (2023) 128–133, https://doi.org/10.1016/j.matpr.2023.04.520.

[69] D. Vo, C. Hwang, K.T. Thi, M. Damtie, M. Liao, HPC produced with CDW as a partial replacement for fine and coarse aggregates using the Densified Mixture Design Algorithm (DMDA) method: Mechanical properties and stability in development, Constr. Build. Mater. (2020) 121441, https://doi.org/10.1016/j.conbuildmat.2020.121441.

[70] Z. Yuan, Y. Jia, Mechanical properties and microstructure of glass fiber and polypropylene fiber reinforced concrete: An experimental study, Constr. Build. Mater. 266 (2021) 121048, https://doi.org/10.1016/j.conbuildmat.2020.121048.

[71] P. Lokesh, T.S.A. Surya Kumari, R. Gopi, G.B. Loganathan, A study on mechanical properties of bamboo fiber reinforced polymer composite, Mater. Today Proc. 22 (xxxx) (2020) 897–903, https://doi.org/10.1016/j.matpr.2019.11.100.

[72] R. Abdulwahab, B.D. Ikotun, A.A. Raheem, E.A. Adetoro, O.K. Oriti, Supplementary cementitious influence of cashew leaf ash as cement replacement in the production of mortar, J. Build. Pathol. Rehabil. 10 (2) (2025) 1–11, https://doi.org/10.1007/s41024-025-00624-6.

[73] B.S. Institution, BS EN 1015 - 11: Methods of Test for Mortar- Part 11: determination of flexural and compressive strength of hardened mortar, BSI Stand. Publ. (2019) 1–15.

[74] American Society for Testing & Materials, ASTM C348 – standard test method for flexural strength of hydraulic-cement mortars, Annu. B. ASTM Stand ! (2021) 1–5.

[75] American Society for Testing & Materials, ASTM C349 - standard test method for compressive strength of hydraulic-cement mortars (using portions of prisms broken in flexure), Am. Soc. Test. Mater. (2018) 1–4.

[76] I. Standard, IS 13311 (Part 1) - Method of Non-destructive testing of concret, Part 1: ultrasonic pulse velocity, Bur. Indian Satandards (2018) 1–7.

[77] D. Vo, C. Hwang, M. Damtie, M. Liao, The influence of MgO addition on the performance of alkali-activated materials with slag À rice husk ash blending, J. Build. Eng. 33 (January 2020) (2021) 101605, https://doi.org/10.1016/j.jobe.2020.101605.

[78] C. Hwang, M. Damtie, D. Vo, T. Huynh, Development of high-strength alkali-activated pastes containing high volumes of waste brick and ceramic powders, Constr. Build. Mater. 218 (2019) 519–529, https://doi.org/10.1016/j.conbuildmat.2019.05.143.

[79] V.H.J.M. dos Santos, et al., Application of Fourier Transform infrared spectroscopy (FTIR) coupled with multivariate regression for calcium carbonate (CaCO3) quantification in cement, Constr. Build. Mater. 313 (October) (2021), https://doi.org/10.1016/j.conbuildmat.2021.125413.

[80] H. Zhang, Y. Xu, Y. Gan, Z. Chang, E. Schlangen, B. Šavija, Microstructure informed micromechanical modelling of hydrated cement paste: Techniques and challenges, Constr. Build. Mater. 251 (2020) 118983, https://doi.org/10.1016/j.conbuildmat.2020.118983.

[81] D. Nath, K. Jangid, A. Susaniya, R. Kumar, R. Vaish, Eggshell derived CaO-Portland cement antibacterial composites, Compos. Part C. Open Access 5 (ember 2020) (2021) 100123, https://doi.org/10.1016/j.jcomc.2021.100123.

[82] X. Ding, et al., Investigating the Hydration, Mechanical Properties, and Pozzolanic Activity of Cement Paste Containing Co-Combustion Fly Ash, Buildings 14 (5) (2024), https://doi.org/10.3390/buildings14051305.

[83] C. Hwang, D. Vo, V. Tran, M. Damtie, Effect of high MgO content on the performance of alkali-activated fine slag under water and air curing conditions, Constr. Build. Mater. 186 (2018) 503–513, https://doi.org/10.1016/j.conbuildmat.2018.07.129.

[84] A. Qudoos, H.G. Kim, Atta-ur-Rehman, J.S. Ryou, Effect of mechanical processing on the pozzolanic efficiency and the microstructure development of wheat straw ash blended cement composites, Constr. Build. Mater. 193 (2018) 481–490, https://doi.org/10.1016/j.conbuildmat.2018.10.229.

[85] G.C. Cordeiro, R.D. Toledo Filho, L.M. Tavares, E.D.M.R. Fairbairn, S. Hempel, Influence of particle size and specific surface area on the pozzolanic activity of residual rice husk ash, Cem. Concr. Compos 33 (5) (2011) 529–534, https://doi.org/10.1016/j.cemconcomp.2011.02.005.

[86] S.A. Bernal, J.L. Provis, V. Rose, R. Mejía De Gutierrez, Evolution of binder structure in sodium silicate-activated slag-metakaolin blends, Cem. Concr. Compos 33 (1) (2011) 46–54, https://doi.org/10.1016/j.cemconcomp.2010.09.004.

[87] S.A. Memon, S. Khan, I. Wahid, Y. Shestakova, M. Ashraf, Evaluating the Effect of Calcination and Grinding of Corn Stalk Ash on Pozzolanic Potential for Sustainable Cement-Based Materials, Adv. Mater. Sci. Eng. 2020 (2020), https://doi.org/10.1155/2020/1619480.

[88] N.M. Khalil, E.M. Hassan, M.M.E. Shakdofa, M. Farahat, Beneficiation of the huge waste quantities of barley and rice husks as well as coal fly ashes as additives for Portland cement, J. Ind. Eng. Chem. 20 (5) (2014) 2998–3008, https://doi.org/10.1016/j.jiec.2013.11.034.

[89] A. Schackow, D. Stringari, L. Senff, S.L. Correia, A.M. Segadães, Influence of fired clay brick waste additions on the durability of mortars, Cem. Concr. Compos 62 (2015) 82–89, https://doi.org/10.1016/j.cemconcomp.2015.04.019.

[90] M.D. Yehualaw, C.L. Hwang, D.H. Vo, A. Koyenga, Effect of alkali activator concentration on waste brick powder-based ecofriendly mortar cured at ambient temperature, J. Mater. Cycles Waste Manag 23 (2) (2021) 727–740, https://doi.org/10.1007/s10163-020-01164-6.

[91] J. Ma, H. Zhang, D. Wang, H. Wang, G. Chen, Rheological properties of cement paste containing ground fly ash based on particle morphology analysis, Crystals 12 (4) (2022), https://doi.org/10.3390/cryst12040524.

[92] N.K. Lee, E.M. Kim, H.K. Lee, Mechanical properties and setting characteristics of geopolymer mortar using styrene-butadiene (SB) latex, Constr. Build. Mater. 113 (2016) 264–272, https://doi.org/10.1016/j.conbuildmat.2016.03.055.

[93] D. Vo, M. Damtie, C. Hwang, M. Liao, Mechanical and durability properties of recycled aggregate concrete produced from recycled and natural aggregate blended based on the Densified Mixture Design Algorithm method, J. Build. Eng. 35 (December 2020) (2021) 102067, https://doi.org/10.1016/j.jobe.2020.102067.

[94] M. Mastali, P. Kinnunen, A. Dalvand, R. Mohammadi Firouz, M. Illikainen, Drying shrinkage in alkali-activated binders – A critical review, Constr. Build. Mater. 190 (2018) 533–550, https://doi.org/10.1016/j.conbuildmat.2018.09.125.
[95] O.A. Mohamed, H.A. Zuaiter, M. M. Jawa, Carbonation and chloride penetration resistance of sustainable structural concrete with alkali-activated and ordinary Portland cement binders: a critical review, Sustain. Struct. 5 (2) (2025) 1–29, https://doi.org/10.54113/j.sust.2025.000075.
[96] L. Wang, F. Aslani, Electrical resistivity and piezoresistivity of cement mortar containing ground granulated blast furnace slag, Constr. Build. Mater. 263 (2020) 120243, https://doi.org/10.1016/j.conbuildmat.2020.120243.